Atmos. Chem. Phys., 25, 119–142, 2025
https://doi.org/10.5194/acp-25-119-2025

Atmospheric Chemistry and Physics
Open Access
EGU

Potential impacts of marine fuel regulations on an Arctic stratocumulus case and its radiative response

Luís Filipe Escusa dos Santos[1,a], Hannah C. Frostenberg[2], Alejandro Baró Pérez[2], Annica M. L. Ekman[3,4], Luisa Ickes[2], and Erik S. Thomson[1]

[1]Department of Chemistry and Molecular Biology, University of Gothenburg, Gothenburg, Sweden
[2]Department of Space, Earth, and Environment, Chalmers University of Technology, Gothenburg, Sweden
[3]Department of Meteorology, Stockholm University, Stockholm, Sweden
[4]Bolin Centre for Climate Research, Stockholm, Sweden
[a]now at: Department of Space, Earth, and Environment, Chalmers University of Technology, Gothenburg, Sweden

Correspondence: Luís Filipe Escusa dos Santos (luis.santos@chalmers.se) and Luisa Ickes (luisa.ickes@chalmers.se)

Received: 20 June 2024 – Discussion started: 27 June 2024
Revised: 11 September 2024 – Accepted: 2 October 2024 – Published: 7 January 2025

Abstract. Increased surface warming over the Arctic triggered by increased greenhouse gas concentrations and feedback processes in the climate system has been causing a steady decline in sea-ice extent and thickness. With the retreating sea ice, shipping activity will likely increase in the future, driven by economic activity and the potential for realizing time and fuel savings from using shorter trade routes. Moreover, over the last decade, the global shipping sector has been subject to regulatory changes that affect the physicochemical properties of exhaust particles. International regulations aiming to reduce SO_x and particulate matter (PM) emissions mandate ships to burn fuels with reduced sulfur content or, alternatively, use wet scrubbing as an exhaust aftertreatment when using fuels with sulfur contents exceeding regulatory limits. Compliance measures affect the physicochemical properties of exhaust particles and their cloud condensation nucleus (CCN) activity in different ways, with the potential to have both direct and indirect impacts on atmospheric processes such as the formation and lifetime of clouds. Given the relatively pristine Arctic environment, ship exhaust particle emissions could cause a large perturbation to natural baseline Arctic aerosol concentrations. Low-level stratiform mixed-phase clouds cover large areas of the Arctic region and play an important role in the regional energy budget. Results from laboratory marine engine measurements, which investigated the impact of fuel sulfur content (FSC) reduction and wet scrubbing on exhaust particle properties, motivate the use of large-eddy simulations to further investigate how such particles may influence the micro- and macrophysical properties of a stratiform mixed-phase cloud case observed during the Arctic Summer Cloud Ocean Study campaign. Simulations with diagnostic ice crystal number concentrations revealed that enhancement of ship exhaust particles predominantly affected the liquid-phase properties of the cloud and led to decreased liquid surface precipitation, increased cloud albedo, and increased longwave surface warming. The magnitude of the impact strongly depended on ship exhaust particle concentration, hygroscopicity, and size, where the effect of particle size dominated the impact of hygroscopicity. While low-FSC exhaust particles were mostly observed to affect cloud properties at exhaust particle concentrations of $1000\,cm^{-3}$, exhaust wet scrubbing already led to significant changes at concentrations of $100\,cm^{-3}$. Additional simulations with the cloud ice water path increased from ≈ 5.5 to $\approx 9.3\,g\,m^{-2}$ show more-muted responses to ship exhaust perturbations but revealed that exhaust perturbations may even lead to a slight radiative cooling effect depending on the microphysical state of the cloud. The regional impact of shipping activity on Arctic cloud properties may, therefore, strongly depend on ship fuel type, whether ships utilize wet scrubbers, and ambient thermodynamic conditions that determine prevailing cloud properties.

Published by Copernicus Publications on behalf of the European Geosciences Union.

1 Introduction

Maritime shipping is a significant source of atmospheric pollutants with wide-ranging impacts on human health (Corbett et al., 2007; Jonson et al., 2020; Liu et al., 2016) and the climate system (Lauer et al., 2007; Eyring et al., 2010; Lund et al., 2012, 2020). Quantifying the net impact of ship exhaust emissions on Earth's radiative budget is a challenging task due to large spatial variability in atmospheric conditions and heterogeneity in air exhaust composition. While ships emit a substantial amount of greenhouse gases, such as CO_2, the remaining constituents can vary substantially with the propulsion system and fuel type used by the individual vessel (Lack et al., 2009; Lack and Corbett, 2012; Lehtoranta et al., 2019). While CO_2 emissions contribute to climate warming, the overall impact of particulate matter and SO_2 exhaust emissions is subject to a much larger uncertainty envelope.

Ship exhaust emissions of primary and secondary particles have been identified as leading to tens of thousands of premature deaths worldwide (Corbett et al., 2007). Regions that are particularly affected by these emissions include coastal areas and port cities with high-population densities, including parts of Europe and East Asia. Motivated by the harmful effects that ship exhaust particles have for human health, the International Maritime Organization (IMO) decided to introduce international marine fuel regulations, which primarily target a reduction in sulfur oxides (SO_x). These regulations mandate that ship operators use marine fuels with fuel sulfur content (FSC) lower than 0.5 wt %, effective globally, and lower than 0.1 wt % in designated sulfur emission control areas (SECA) or utilize exhaust treatment systems to reduce emissions (IMO, 2008). Since low-FSC fuels are generally associated with a higher cost than conventional fuel, high-FSC residual fuel oil (UNCTAD, 2022) wet-scrubbing systems pose an economically attractive treatment alternative, which allows stakeholders to continue to use marine fuels with FSCs exceeding regulatory limits (IMO, 2008). Wet scrubbers are exhaust aftertreatment systems that utilize seawater mist or chemically treated freshwater to remove SO_x from ship exhaust and thus prevent the formation of sulfur-containing secondary aerosol particles (Oikawa et al., 2003; Andreasen and Mayer, 2007). While recent studies demonstrate that utilization of low-FSC marine fuels generally reduces the number of particles emitted by ships (Zetterdahl et al., 2016; Kuittinen et al., 2021; Seppälä et al., 2021), the impact of wet scrubbing on particle exhaust emissions is less well understood and subject to large variability (Fridell and Salo, 2016; Lehtoranta et al., 2019; Winnes et al., 2020; Yang et al., 2021; Jeong et al., 2023). Moreover, compliance alternatives, such as exhaust aftertreatment systems, have been found to affect the physicochemical properties of exhaust particles in different ways, which also have implications for atmospheric processes and the net climate effect of shipping activity. Combustion of low-FSC fuels often results in the emission of predominantly hydrophobic soot particles, leading to reduced emissions of cloud condensation nuclei (CCNs) compared to higher CCN emissions from conventional, high-FSC fuel combustion (Lack et al., 2009; Yu et al., 2020, 2023). In contrast, wet scrubbing has been found to alter the physicochemical properties of the particle emissions (Lieke et al., 2013; Santos et al., 2023, 2024). This can yield larger fractions of water-soluble content in the exhaust particle phase and cause a shift in particle size distributions to larger particles compared to exhaust particle emissions from conventional, high-FSC fuel combustion. Combustion particles from wet scrubbing require relatively low supersaturations to be activated into liquid droplets (Santos et al., 2023), which can lead to enhanced CCN number emissions at given supersaturations (Santos et al., 2023, 2024).

Shipping emissions are currently estimated to have a net cooling effect on the climate; higher exhaust particle number concentrations can lead to increased cloud reflectivity, which dominates the warming effect of shipping-related CO_2 emissions (Lauer et al., 2007; Eyring et al., 2010; Lund et al., 2012, 2020). Ship tracks are the visible manifestation of ship exhaust perturbations on cloud properties, resulting in persistent, regionally constrained marine stratiform cloud features with increased cloud albedo (Coakley et al., 1987; Hobbs et al., 2000; Possner et al., 2018). The extent of ship tracks depends on the background state of the boundary layer, including meteorological parameters, the cloud fraction, and aerosol particle and CCN number concentrations (Coakley et al., 1987; Durkee et al., 2000; Hobbs et al., 2000). Observations along the coast of California have shown that the 0.1 wt % FSC limit, introduced in 2015 in SECAs, led to strong reductions in visible ship track formation (Gryspeerdt et al., 2019; Watson-Parris et al., 2022). While ship sulfate emissions are one key driver of ship track formation, FSC reduction policies may still lead to cloud perturbations. These cloud perturbations may be undetectable to some analysis techniques, resulting in an underestimate of shipping-induced radiative forcing (Gryspeerdt et al., 2019; Manshausen et al., 2022). With the introduction of the global 0.5 wt % FSC cap in 2020 and associated implications for exhaust particles, radiative cooling induced by ship exhaust emissions may diminish. Studies investigating the impact of the 2020 0.5 wt % FSC cap have reported lower ship track formation frequencies and highlight the reduction in SO_2 emissions as key drivers of this observation (Gryspeerdt et al., 2019; Yuan et al., 2022; Watson-Parris et al., 2022). Therefore, IMO FSC regulations may imply diminished radiative cooling from shipping emissions. However, the magnitude of diminished cooling may be subject to a systematic underestimate, as ship track visibility is strongly dependent on the cloud background states (Gryspeerdt et al., 2019; Yuan et al., 2022; Watson-Parris et al., 2022).

One region where future shipping activity might lead to strong climate feedback is the Arctic. The Arctic is experiencing unprecedented amplified surface warming compared to the global average, caused by a complex system of interacting processes within its climate system (Serreze and Francis, 2006; Serreze and Barry, 2011; Rantanen et al., 2022). Low-level mixed-phase clouds play a key role in the Arctic climate system (Morrison et al., 2012). While low-level clouds generally lead to surface cooling, they tend to enhance surface warming in the Arctic throughout most of the year by trapping and re-emitting longwave radiation (Intrieri et al., 2002; Shupe and Intrieri, 2004). Enhanced surface warming in the Arctic promotes ice and snow melting and as a consequence, Arctic sea-ice extent and thickness have been in decline for the past decades (Screen and Simmonds, 2010; Serreze and Barry, 2011). This will likely grant ships easier access to exploration and extraction of natural resources and may enable the use of shorter trading routes through Arctic waterways, deviating from the more conventional and longer routes through the Suez and Panama canals. The economic feasibility of Arctic shipping routes compared to traditional routes is debated (Lasserre and Pelletier, 2011). Nonetheless, shipping activity and related exhaust emissions are expected to increase significantly within the near future (Corbett et al., 2010; Paxian et al., 2010; Peters et al., 2011). In the Arctic, ambient particle number concentrations are relatively low compared to other regions of the Earth, and thus relatively small absolute increases in aerosol concentrations can substantially impact cloud formation and properties (Mauritsen et al., 2011; Bulatovic et al., 2021). Ship emissions may therefore become a strong, localized aerosol source that could alter the properties of Arctic clouds and thereby the radiative budget.

Several studies have investigated the potential impacts of increased Arctic shipping activity on Arctic cloud properties (Christensen et al., 2014; Possner et al., 2017; Gilgen et al., 2018; Eirund et al., 2019). Ship aerosol emissions were observed to generate a shift towards the ice phase, reducing precipitation and increasing cloud albedo (Christensen et al., 2014; Possner et al., 2017). Possner et al. (2017) observed a noteworthy rise in liquid water content (LWC) when ship-emitted CCNs surpassed $1000\,\mathrm{cm}^{-3}$. However, results determining whether ship-emission-related changes were sufficient to impact Arctic warming rates were inconclusive (Christensen et al., 2014; Possner et al., 2017). Gilgen et al. (2018) modeled significant impacts on Arctic cloud properties from shipping when exaggerated future Arctic ship emission inventories were used, i.e., when Arctic shipping emissions for 2050 were increased by a factor of 10. In contrast, Stephenson et al. (2018) investigated the total climate impact from trans-Arctic shipping and found an increase in total cloud fraction and the cloud liquid water path (LWP) due to CCN enhancements from ship emissions, diminishing Arctic warming rates and exerting cooling rates on the order of 1 °C by the end of the 21st century. Eirund et al. (2019) highlight how underlying surfaces influence the properties of mixed-phase clouds, and thus the impact of additional CCNs from ship exhaust emissions may be weakened or strengthened, depending on the ice cover.

Ship exhaust emissions also have the potential to exert radiative forcing via direct interactions between emitted particles and solar radiation or via a reduction in the surface albedo due to deposition of light-absorbing black carbon (BC) particles onto snow. A modeling study by Dalsøren et al. (2013) examined a number of direct and indirect processes related to shipping emissions and radiative processes. The study found significant seasonal variability in all processes and that direct sulfate–aerosol interactions exert the largest radiative forcing (positive) out of all processes, i.e., a larger forcing than aerosol–cloud interactions. Given IMO's marine fuel policies, the impact of ship-related sulfate contributions may be subject to large uncertainties. In contrast, Gilgen et al. (2018) and Stephenson et al. (2018) found that radiative forcing induced by aerosol–cloud interactions outweighs the forcing exerted by direct aerosol–radiation interaction and BC deposition onto snow. Similarly, Browse et al. (2013) and Li et al. (2021) report only minor contributions of BC deposition from shipping activity, which would yield insignificant changes in radiative forcing and would not contribute to accelerated sea-ice loss. While these findings apply for the Arctic in general, surface albedo adjustments due to BC deposition may have stronger locally constrained impacts, for example, in the sub-Arctic region (Browse et al., 2013).

The aim of our study is to investigate how ship exhaust particle perturbations influence the microphysical structure of an Arctic mixed-phase cloud and thereby its climate effect. We elaborate on the differences in different ship exhausts based on laboratory results (Santos et al., 2022, 2023, 2024). In this study, we use large-eddy simulation (LES) to simulate a well-characterized mixed-phase stratocumulus cloud observed during the Arctic Summer Cloud Ocean Study (ASCOS) campaign (Tjernström et al., 2012, 2014). We systematically perturb the aerosol concentrations in the model domain to explore the effect of different types of ship exhausts. While previous studies investigating cloud perturbations caused by ship exhaust emissions used simplistic representations of physicochemical properties of ship exhaust particles, herein we utilize detailed exhaust particle information obtained from laboratory marine engine experiments, where the impact of FSC reduction and exhaust wet scrubbing on ship exhaust particle properties was examined (Santos et al., 2022, 2023, 2024). The model is initially run with an ambient background aerosol concentration only. Subsequent model simulations utilize several potential ship aerosol concentrations with different particle size distributions, densities, and hygroscopicities, mirroring the effects of FSC reduction and wet scrubbing. We evaluate the role of ship aerosol properties in affecting the cloud LWP and ice water path (IWP) and the concentration of cloud droplets and raindrops. The results

are used to calculate changes in surface precipitation, cloud drop effective radius, cloud albedo, and other cloud properties, which have implications for the radiative surface budget. Potential Arctic climate feedbacks from increased shipping activity, in the context of the adaption of different fuel types and propulsion technologies by ships, are discussed.

2 Methods

2.1 Laboratory pre-study – physicochemical properties of ship exhaust aerosol

The experimental results used in this study are based on a series of laboratory experiments that were performed between 2019 and 2022 in Gothenburg, Sweden. More details on the laboratory experiments can be found in Santos et al. (2022, 2023, 2024). Engine experiments were performed using stationary marine test-bed diesel engines, fuel types of varying sulfur content, a laboratory wet scrubber, and a range of gas and aerosol instrumentation for quantifying physicochemical properties of exhaust particles. For the simulations with the MISU–MIT Cloud and Aerosol (MIMICA) LES model, the following parameters are needed as input to describe the aerosol perturbation: particle size distributions, particle effective densities, and hygroscopicities. Particle size distributions were measured using scanning mobility particle sizers (SMPS). We describe the average particle size distributions using the count median diameter (CMD) and the geometric standard deviation (σ_g). Effective particle densities (ρ_{eff}) were determined by coupled SMPS and aerodynamic aerosol classifier (AAC) measurements and calculated following Tavakoli and Olfert (2014) and Santos et al. (2022, 2024). Exhaust particle hygroscopicities (κ) were determined from size-selected CCN measurements using a CCN counter (CCNc; CCN-100, Droplet Measurement Technologies; Roberts and Nenes, 2005) and from parameterizations by Petters and Kreidenweis (2007).

From Santos et al. (2022, 2023), we use results from measurements with high-FSC fuel (HiS; HGO in the respective studies), one low-FSC fuel (LoS; MGO in the respective studies), and seawater scrubbing experiments performed in combination with HiS fuel combustion (WS; SWS in the respective studies). For the LES experiments, the results were simplified by assigning identical size distributions to HiS and LoS, which did not display substantial differences during the respective measurement campaigns. The particle size distributions used in the model are shown in Fig. 1a. Other results such as average case-dependent ρ_{eff} and κ values, which were used as input parameters, are listed in Table 1 and discussed further in Sect. 2.3.

Engine experiments summarized in Santos et al. (2024) utilized a different engine with a higher power output and fuels with different properties compared to Santos et al. (2022, 2023) and therefore resulted in different emission characteristics. From Santos et al. (2024), only results obtained for high-FSC fuel combustion and exhaust wet scrubbing at engine load points of 50 % were implemented in this study. Both cases resulted in emissions of bimodal size distributions consisting of a dominant, hygroscopic sulfate mode and a smaller, relatively hydrophobic soot mode. Here, corresponding bimodal particle size distributions were simplified to the respective unimodal hygroscopic sulfate modes. The dominant sulfate modes (Fig. 1b) with their respective averaged ρ_{eff} and κ values are summarized in Table 1. The

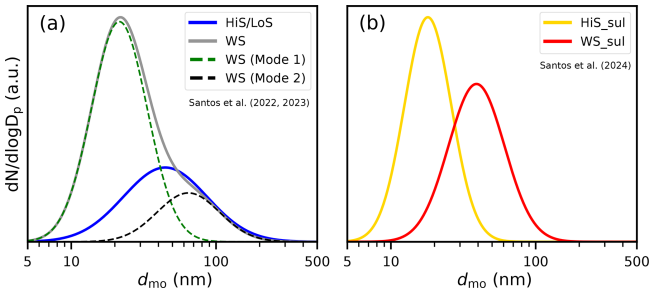

Figure 1. **(a)** Particle size distributions of high-FSC (HiS) and low-FSC (LoS) fuel and wet-scrubbed (WS) exhaust particles from Santos et al. (2022, 2023) and **(b)** the sulfate particle modes of HiS fuel (HiS_sul) and scrubbed exhaust particles (WS_sul) from Santos et al. (2024). The dashed lines in panel **(a)** represent the two individual modes of the bimodal WS case. The data shown in the figure represent size distributions measured during the respective measurement campaigns that have been averaged and simplified to be parameterized within MIMICA.

Table 1. Properties of marine background (BG) and ship aerosol used as model input parameters, including the count median diameter (CMD) and geometric standard deviation (σ_g) of the size distributions, particle density (ρ_{eff}), and aerosol hygroscopicity (κ). HiS, LoS, and WS data were obtained from experiments outlined in Santos et al. (2022, 2023) and refer to the combustion of high- (HiS) and low-FSC fuels (LoS) and wet-scrubbed HiS exhaust (WS). HiS_sul and WS_sul represent the sulfate particle modes measured for high-FSC fuel and wet-scrubbed exhaust in Santos et al. (2024), respectively. The WS case is composed of a bimodal distribution; hence, the two separate aerosol modes are listed in the table. For each ship exhaust sensitivity test, two sets of simulations with low or high ship aerosol number concentrations were performed. Corresponding simulations with low and high concentrations (N_p) are additionally labeled with _lo and _hi, respectively.

Case	CMD [nm]	σ_g	ρ_{eff} [g cm^{-3}]	κ	N_p [cm^{-3}]
BG (Aitken)	32	1.1	2.18	1	30
BG (acc)	93	1.5	2.18	1	30
LoS	45	1.6	0.91	0.04	100/1000
HiS	45	1.6	1.02	0.11	100/1000
WS (mode 1)	22	1.2	1.18	0.22	131.3/1313
WS (mode 2)	64	1.3	1.09	0.16	36.7/367
HiS_sul	18	1.15	1.6	0.64	100/1000
WS_sul	39	1.22	1.6	0.64	100/1000

high-FSC case is referred to as HiS_sul and the seawater wet-scrubbing case as WS_sul.

The main findings from Santos et al. (2022, 2023) showed that FSC reduction and exhaust wet scrubbing led to substantial impacts on particulate emissions from ship engines. A switch to marine fuels with reduced FSC did not significantly affect particle size distributions and total number emissions but decreased the exhaust particle ρ_{eff} and κ values. On the other hand, wet scrubbing was found to lead to the formation of a dominant particle mode around 20 nm and to increased ρ_{eff} and κ values due to changes in the chemical mixing state. Similarly, Santos et al. (2024) investigated the impact of different fuel types and seawater exhaust wet scrubbing on exhaust particle properties but used a different test-bed engine with a higher total power output. One key difference compared to Santos et al. (2022, 2023) was that the combustion of non-compliant high-FSC fuel resulted in bimodal particle size distributions with a dominant sulfate mode around 20 nm. When the high-FSC fuel exhaust was scrubbed, the sulfate mode shifted towards larger sizes, likely due to the coagulation of particles inside the scrubber.

2.2 MIMICA model description and case setup

LES experiments were conducted with the MIMICA model. This model was originally designed to study high-latitude mixed-phase clouds and has been thoroughly documented and evaluated against observations (see, e.g., Savre et al., 2015; Stevens et al., 2018; Bulatovic et al., 2023). Herein only a brief description of the model is provided. For more detailed information, see Savre et al. (2014).

MIMICA solves a set of anelastic, non-hydrostatic governing equations and uses a two-moment bulk microphysics scheme to predict the mass-mixing ratios (Q) and number densities (N) of five hydrometeor classes, including cloud droplets, raindrops, ice crystals, graupel, and snow. Growth of liquid-phase hydrometeors via auto-conversion, self-collection, and collision–coalescence are treated following Seifert and Beheng (2001) and Seifert and Beheng (2006). Interactions between liquid- and ice-phase hydrometeors are treated according to the two-moment bulk microphysics by Wang and Chang (1993). Hygroscopic growth of aerosol particles and activation into cloud droplets is calculated according to the κ-Köhler theory (Petters and Kreidenweis, 2007). While MIMICA does include options for heterogeneous ice nucleation, here diagnostic ice crystal number concentrations (N_{i}) are utilized as in Ovchinnikov et al. (2011, 2014). This means that in grid cells where the temperature (T) is less than 0 °C and sufficient supercooled cloud water is present ($Q_{\text{c}} \geq 2\times10^{-7}$ g m^{-3}), N_{i} is relaxed towards a pre-determined constant value. As a default, this value for N_{i} was set to 200 m^{-3} based on the control simulations in Stevens et al. (2018). The decision to use a constant diagnostic N_{i} instead of an interactive heterogeneous ice nucleation scheme was motivated by findings showing that typical engine exhaust particles, such as BC, are inefficient ice nucleators in the immersion freezing regime (Mahrt et al., 2018; Kanji et al., 2020). In addition, Santos et al. (2024) found no significant differences in the ice nucleation behavior of exhaust particles emerging from low- and high-FSC fuel combustion and from exhaust wet scrubbing.

The simulated stratocumulus case is based on observations made during ASCOS on 31 August 2008 at approximately 87° N, 11° W (see Appendix A for the detailed vertical profiles used to initialize the model; Tjernström et al., 2012, 2014). Note that the meteorological conditions from ASCOS were only used to initialize the model. Potential temperature and total water mixing ratio are prognostic variables influenced by sources and sinks in the model (e.g., radiation, microphysical phase changes, and precipitation) but do not necessarily represent the temporal evolution of the real atmospheric state. The case study represents a stable mixed-phase cloud that has previously been investigated using MIMICA (Igel et al., 2017; Stevens et al., 2018; Christiansen et al., 2020; Sotiropoulou et al., 2021; Frostenberg et al., 2023). For more details on the setup of MIMICA, please see the aforementioned references, and for more extensive information on the ASCOS campaign and the experimental results, see Tjernström et al. (2012, 2014).

The MIMICA 3-D domain consists of $96 \times 96 \times 128$ grid cells with periodic boundaries. The horizontal resolution is uniform ($\mathrm{d}x = \mathrm{d}y = 62.5$ m), while the grid spacing in the vertical z direction is variable (7.5 m $\leq \mathrm{d}z \leq$ 25 m). A higher vertical resolution is applied to grid cells near the surface and within the cloud layer, whereas a sinusoidal function is used to define the vertical spacing of grid cells at other altitudes. The total domain is 6 km × 6 km in the horizontal direction and 1.7 km in the vertical direction. All simulations were run for 16 h. The first 4 h are considered to be spin-up and are thus excluded from the presented results.

The radiation solver used in this study is based on Fu and Liou (1992). It is important to note that while radiation is affected by cloud hydrometeors, it is not affected by aerosols. Surface temperature and pressure have prescribed values of 269.8 K and 1026.3 hPa, respectively. The surface albedo is set to 0.844 and the surface roughness to 0.0004 m. Sensible and latent heat fluxes at the surface are both set to 0 W m^{-2} based on the small values reported in Tjernström et al. (2014). A large-scale divergence of 1.5×10^{-6} s^{-1} is imposed over the whole domain. Large-scale advection is turned off in the model.

Additional simulations of no_ship, HiS_sul, and WS_sul were performed with N_{i} increased from 200 to 600 m^{-3}. The aim of these additional simulations was to investigate the susceptibility of a thinner mixed-phase cloud, i.e., with reduced LWP and cloud depth, to ship exhaust particle perturbations. A maximum value of $N_{\text{i}} = 600$ m^{-3} induced a sufficiently large reduction in LWP to perform the aforementioned sensitivity tests, and simultaneously, simulated LWP and IWP values agree well with observational data (see Sect. 3.4). Addi-

tional testing revealed that further increases in N_i would lead to dissipation of the cloud. Associated model runs are named after previous model runs but with an appended _ni600, e.g., no_ship_ni600.

2.3 Aerosol implementation in MIMICA

Aerosol particles in MIMICA were represented as aerosol modes that follow lognormal distributions, described by a CMD and σ_g. Values of the aerosol effective density ρ_{eff}, the aerosol hygroscopicity expressed via κ, and the aerosol number concentrations (N_p) were assigned to each aerosol mode. For all simulations, aerosol number concentrations and properties were set to be uniform and constant in time over the entire 3-D domain. Aerosol particles can be activated into cloud droplets according to κ-Köhler theory but are modeled without additional sources and sinks during the simulations. Several aerosol modes can co-exist. In our simulations, we describe the total aerosol using natural background aerosol modes and ship exhaust aerosol modes (for the cases with additional ship exhaust particles).

Natural background (BG) aerosol concentrations were present in all model runs (Table 1). These BG aerosols were assumed to have hygroscopicity values in agreement with marine sea spray ($\kappa = 1$) and were included in both the Aitken and accumulation (acc) modes. The N_p of the BG aerosol was chosen to be $30\,cm^{-3}$ in both modes based on aerosol measurements during the ASCOS expedition (Kupiszewski et al., 2013). In the baseline simulation (referred to as no_ship), only BG Aitken and acc mode aerosol were present.

For the sensitivity experiments, different aerosol concentrations and types were added to represent different ship exhaust perturbations (HiS, LoS, and WS from Santos et al., 2022, 2023, and HiS_sul and WS_sul from Santos et al., 2024). Ship aerosol properties are summarized in Table 1 and Sect. 2.1. For each case, ship exhaust perturbation experiments were performed at two concentration levels, $N_{p,ship} = 100\,cm^{-3}$ (labeled _lo) and $N_{p,ship} = 1000\,cm^{-3}$ (labeled _hi). An exception is the WS case where the concentration levels are increased by a factor of ≈ 1.7 following the increase in particle number concentration that has been observed in the experiments when using the wet scrubber. This increase in $N_{p,ship}$ was accounted for in the two particle modes comprising the WS case. The same _lo and _hi labeling, signifying the low- and high-concentration simulations, was used for WS cases.

2.4 Calculations of the cloud drop effective radius and cloud albedo

To examine the difference in cloud radiative properties between the simulations, we calculate the effective droplet radius (r_e), cloud optical depth (τ), and cloud albedo (α) from the model output. To calculate the effective cloud droplet radius r_v, we use the relationship suggested by Freud and Rosenfeld (2012), who found that r_e is on average a factor of 1.08 larger than the volume mean cloud droplet radius r_v,

$$r_e \approx 1.08\, r_v. \tag{1}$$

The volume mean cloud droplet radius r_v is defined as

$$r_v = \left(\frac{3}{4}\frac{Q_c}{\pi \rho_w N_c}\right)^{1/3}, \tag{2}$$

where Q_c is the cloud liquid water content, ρ_w is the density of water ($1000\,kg\,m^{-3}$), and N_c is the cloud droplet number concentration. The cloud's optical depth can be approximated by

$$\tau = \frac{3}{2}\frac{LWP}{r_e \rho_w}, \tag{3}$$

where LWP is the liquid water path, i.e., the vertically integrated amount of liquid cloud water, in $kg\,m^{-2}$ (Stephens, 1978). The cloud albedo can be approximated by

$$\alpha = \frac{(1-g)\tau}{1+(1-g)\tau}, \tag{4}$$

where g is the scattering asymmetry factor, i.e., the average value of the cosine of the scattering angle, and equals 0.85 for the scattering of solar radiation by clouds (Meador and Weaver, 1980).

3 Results

3.1 Influence of ship aerosol on LWP and IWP

In Fig. 2, the time evolution of the domain-averaged LWP and IWP are shown for all the simulations in comparison to the observations from the ASCOS campaign. Note that the ASCOS observations used to initialize the model do not change with time during the remaining simulation period. In all simulations, MIMICA simulates an LWP that exceeds the 75th percentile of the observations (Fig. 2a–b), which was also observed by Bulatovic et al. (2021), who used MIMICA to simulate the same ASCOS case. MIMICA was previously reported to generate a greater LWP when prescribed instead of interactive aerosol particle concentrations are used (Stevens et al., 2018). Additional sensitivity tests with reduced LWP are discussed in Sect. 3.4. The addition of ship aerosol tends to increase the LWP of the cloud compared to the reference no_ship case (Fig. 2a–b; Table 2). This effect is found to be dependent on the ship exhaust aerosol concentrations and the hygroscopicity of the ship exhaust aerosol. The LWP increase is most pronounced for sensitivity tests with high ship aerosol concentrations (HiS_hi, WS_hi, and WS_sul_hi), where LWP increases by up to $\approx 13\,\%$. The increase is less pronounced for both LoS cases due to the hydrophobic nature of the added particles ($\kappa = 0.04$). Despite

having comparatively large κ values, both HiS_sul cases do not yield any substantial increase in LWP, suggesting that the ship exhaust aerosol particles are too small (CMD = 18 nm) to induce a pronounced effect. The identified LWP response for the mixed-phase cloud perturbed by ship exhaust agrees with Possner et al. (2017), who reported substantial increases in LWP when ship-related CCN concentrations exceeded $1000\,\mathrm{cm}^{-3}$ in their simulations.

The simulated IWP is close to the 25th percentile of the observations for all simulations (Fig. 2c–d). In contrast to results for the LWP, additional ship exhaust particles have no substantial effect on the modeled IWP, which is due to the implementation of diagnostic N_i, meaning ship aerosol cannot directly impact N_i. However, in our simulations, ship exhaust aerosol can affect the properties of precipitating ice-phase hydrometeors (graupel and snow) by influencing the accretion of hydrometeors and the availability of water vapor. Sporadic spikes in the temporal evolution of IWP are in all cases caused by increased graupel formation rates at the expense of raindrops. Similar features in IWP evolution are reported by Bulatovic et al. (2021), who used MIMICA with a similar setup. Small increases in IWP for some simulations are mainly caused by an increasing graupel number (N_g) and mass concentration (Q_g; Fig. D1).

3.2 Impact of ship aerosol on hydrometeors

The effect of ship exhaust aerosol perturbations on the temporal evolution of cloud hydrometeors and cloud depth is investigated by examining the horizontally averaged number and mass concentrations of cloud droplets (N_c and Q_c) and raindrops (N_r and Q_r). Corresponding contour plots for the reference simulation (no_ship) and all sensitivity simulations with high ship aerosol concentrations (_hi; 1000 or $1680\,\mathrm{cm}^{-3}$ (WS)) are shown in Fig. 3. In addition, each panel features the horizontally averaged cloud bottom and cloud top height, depicted by the dashed black lines.

In general, impacts of ship aerosol particles on liquid-phase hydrometeors are mostly observed in ship aerosol simulations with the highest $N_\mathrm{p,ship}$, in accordance with the results presented in Sect. 3.1. Ice-phase hydrometeors have been excluded from Fig. 3, as changes in ice crystal concentrations remain more or less unaffected due to the prescribed ice parameterization scheme used in this study (see Sect. 2.2), but they can be found in Appendix B. While cloud droplet numbers are evenly distributed within the cloud layer, Q_c is highest near the cloud top, which is typical of stratocumulus clouds with near-adiabatic conditions. The distribution of N_r displays more-dynamic behavior and reaches its maximum after around 8 h of simulation. In contrast to cloud droplets, Q_r is concentrated in the lower regions of the cloud. All simulations show similar cloud depths and evolutions (Fig. 3). After 4 h (spin-up), the clouds have a depth of around 500 m. The cloud depth increases in all simulations and ranges between 535 m (no_ship) and 570 m (WS_sul_hi) at the end of the simulations due to steady increases in cloud top height.

With the addition of ship aerosol, more aerosol particles are activated into cloud droplets, as can be seen from increased N_c values for LoS_hi, HiS_hi, WS_hi, HiS_sul_hi, and WS_hi (Figs. 3 and 4). The largest increase is observed for WS_hi and WS_sul_hi, where the vertically integrated N_c averaged over the last 4 simulation hours increases by $\approx 57\,\%$. Note that Q_c is almost unaffected by the added ship exhaust aerosol due to the low precipitation rates in the no_ship case. Despite the relatively large κ value of HiS_sul_hi ship exhaust particles ($\kappa = 0.64$), N_c and N_r are not strongly affected, even when ship exhaust aerosol concentrations are set to $N_\mathrm{p} = 1000\,\mathrm{cm}^{-3}$. This implies that HiS_sul exhaust particles were too small (CMD = 18 nm) to act as CCNs. The observed increase in N_c is also observed for LoS_hi, suggesting that additional aerosol particles with low hygroscopicity ($\kappa = 0.04$) can impact cloud properties if their CMD is sufficiently large. Differences in modeled N_c between HiS_sul_hi and LoS_hi ship exhaust aerosol imply that the size of aerosol particles plays a more dominant role than particle hygroscopicity in inducing changes in cloud properties. This observation agrees with Christiansen et al. (2020), who simulated the same ASCOS case with background aerosol modes of varying sizes and hygroscopicity values. Therein, the authors found that microphysical cloud properties were not affected by aerosol particle hygroscopicities if accumulation mode particles were present in the model domain (Christiansen et al., 2020).

Vertical profiles of N_c, Q_c, N_r, and Q_r averaged over the last 4 simulation hours reveal a more detailed picture of how ship perturbations affect concentrations of cloud droplets and raindrops (Fig. 4). The sensitivity tests that show substantial increases in N_c also show reduced raindrop formation in the cloud (Figs. 3 and 4). While no_ship produces substantial numbers of raindrops near the cloud top after about 6 to 7 h of simulation, ship cases with high exhaust particle concentrations lead to general reductions in N_r and Q_r by up to 58 % and 63 %, respectively (Figs. 3 and 4). The magnitude of this response is dependent on the CMD and κ, where the CMD effect dominates the cloud response. The strongest reduction in N_r and Q_r is observed for WS_hi and WS_sul_hi, where both quantities are reduced by about 52 % to 58 % (N_r) and 56 % to 63 % (Q_r) compared to no_ship. Results for raindrop formation coincide with a general reduction in r_e for relevant ship exhaust cases. For both WS_hi and WS_sul_hi, r_e is reduced from 16.56 µm (no_ship) to $\approx 14.68\,\mu\mathrm{m}$ (Fig. 5 and Table 2). A reduction in r_e indicates reduced self-collection (autoconversion) and coalescence and accretion of cloud droplets by raindrops or other hydrometeors.

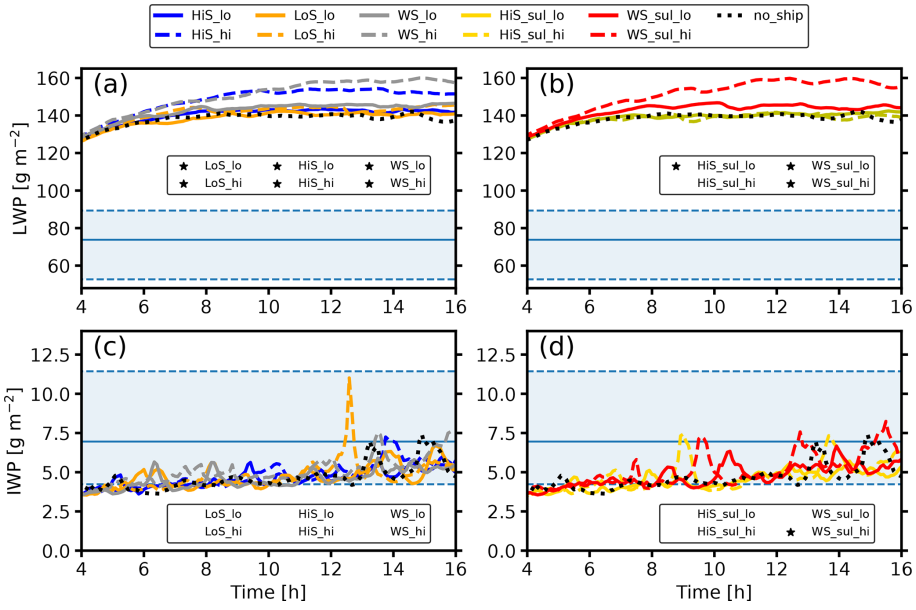

Figure 2. Time evolution of the simulated domain-averaged **(a, b)** liquid water path (LWP) and **(c, d)** ice water path (IWP). no_ship refers to the reference case with background aerosol only. HiS, LoS, and WS represent ship aerosol from measurements of high- and low-sulfur-content fuels and wet scrubbing (Santos et al., 2022, 2023). The HiS_sul and WS_sul cases represent sulfate particle modes of high-FSC fuel combustion and exhaust gas wet scrubbing from Santos et al. (2024). The label additions _lo and _hi signify the ship aerosol concentrations used in the individual model runs. Significant differences between ship exhaust cases and no_ship were assessed using two-sided t tests at a confidence level of 95 %. Model runs with significant differences are marked by star icons in inset legends. For the statistical tests, the last 4 simulation hours were used. The blue-shaded area refers to the retrieved LWP and IWP from microwave radiometer measurements (median over the observation period; the corresponding dashed lines are the 25th and 75th percentiles) during the ASCOS campaign (Tjernström et al., 2012, 2014), which were used to initialize the model. The first 4 h are considered a spin-up period of the model and are removed from the panels.

Table 2. Overview of mean LWP, IWP, surface precipitation rates, cloud effective radius (r_e), cloud albedo (α), and net long- (net LW) and shortwave (net SW) radiation at the surface averaged over the last 4 h of simulation time. Statistical significance, determined by performing two-sided t tests, is highlighted by asterisks. The label additions _lo and _hi signify the ship aerosol concentrations used in the individual model runs.

Case	LWP [g m^{-2}]	IWP [g m^{-2}]	Surface precip. (total) [mm d^{-1}]	Surface precip. (rain) [mm d^{-1}]	r_e [µm]	α	Net LW [W m^{-2}]	Net SW [W m^{-2}]
no_ship	139.3	5.5	0.32	0.06	16.56	0.65	−14.6	6.5
LoS_lo	140.7*	5.3	0.31	0.05	16.50	0.65*	−14.5	6.5
LoS_hi	143.6*	5.5	0.30	0.04*	16.16*	0.66*	−14.4*	6.5
HiS_lo	142.5*	5.1	0.31	0.06	16.41*	0.66*	−14.5	6.5
HiS_hi	152.8*	5.6	0.28*	0.03*	15.41*	0.68*	−14.2*	6.4
WS_lo	145.4*	5.1	0.30	0.06	16.22*	0.66*	−14.4*	6.5
WS_hi	158.6*	5.9	0.27*	0.02*	14.68*	0.70*	−13.9*	6.3
HiS_sul_lo	141.0*	5.0	0.31	0.06*	16.57	0.65*	−14.6	6.5
HiS_sul_hi	139.8	5.4	0.31	0.06	16.52	0.65	−14.6	6.5
WS_sul_lo	144.6*	5.4	0.30	0.05*	16.10*	0.67*	−14.4*	6.5
WS_sul_hi	158.0*	6.2*	0.29	0.02*	14.69*	0.70*	−14.0*	6.3
no_ship_ni600	88.6	9.3	0.35	0.00	15.51	0.57	−17.6	6.9
HiS_sul_lo_ni600	86.6*	9.4	0.36	0.00	15.47*	0.57*	−17.9*	6.9
HiS_sul_hi_ni600	85.8*	9.4	0.35	0.00	15.46*	0.57*	−18.0*	6.9
WS_sul_lo_ni600	88.0*	9.2	0.34	0.00	14.94*	0.58*	−17.9*	6.9
WS_sul_hi_ni600	86.8*	9.6	0.35	0.00	13.59*	0.60*	−17.9*	6.9

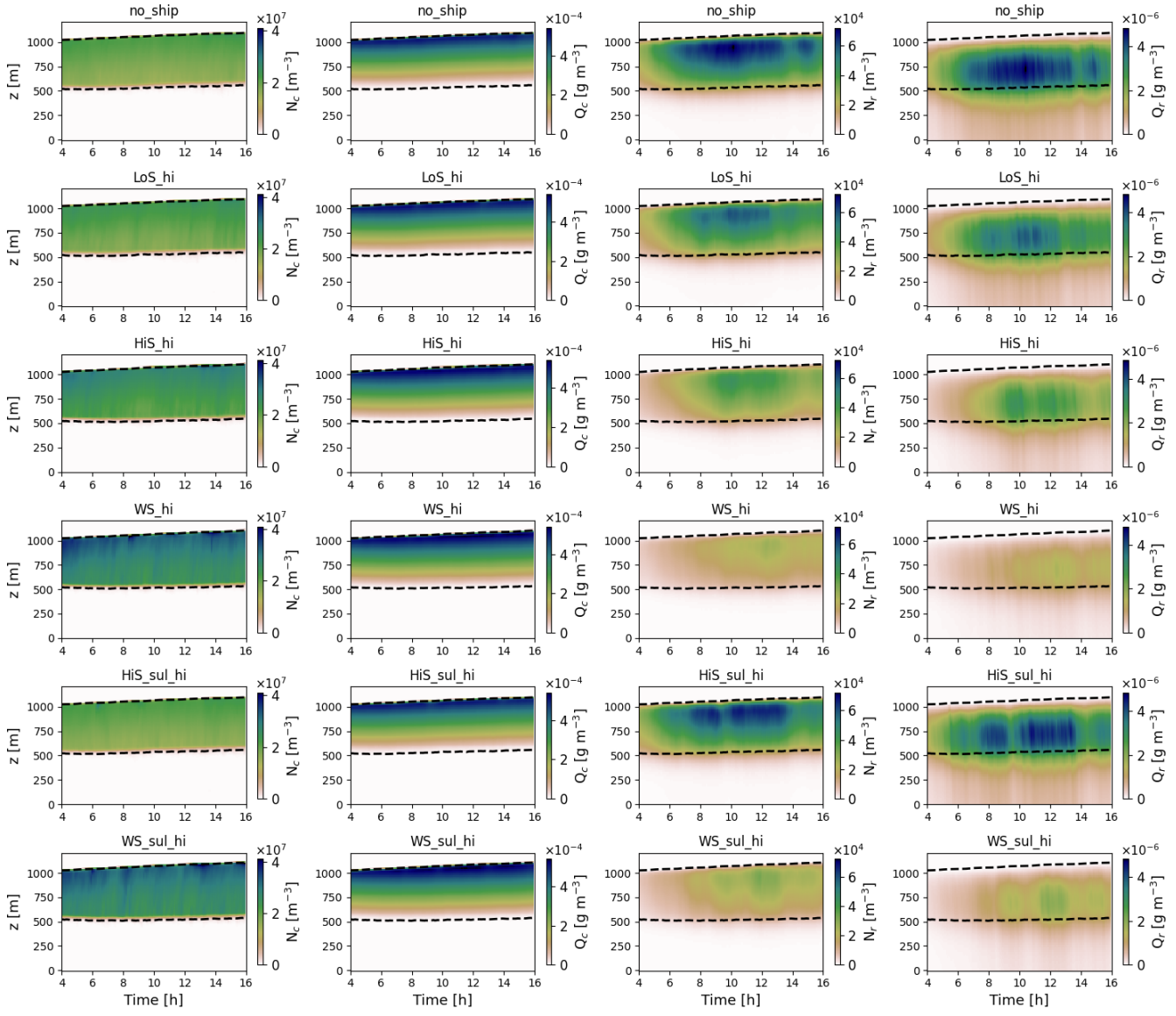

Figure 3. Temporal evolution of horizontal domain-averaged cloud droplet number concentrations (N_c, in m^{-3}), cloud droplet mixing ratios (Q_c, in g m^{-3}), raindrop number concentrations (N_r) and raindrop mixing ratios (Q_r) simulated for the reference case (no_ship) and the high ship aerosol concentration cases LoS_hi, HiS_hi, WS_hi, HiS_sul_hi, and WS_sul_hi. The dashed black lines represent case-specific horizontally averaged cloud bottom and cloud top heights. The spin-up period (0 to 4 h) is removed from all panels.

3.3 Impact of ship aerosol on surface precipitation and cloud radiative properties

The sensitivity tests that led to reductions in N_r and Q_r were not found to impact total surface precipitation rates compared to no_ship (Fig. 5a–b). The majority of surface precipitation is dominated by graupel, which was not found to be affected by the addition of ship exhaust aerosol. Liquid rain typically constitutes less than 5 % of the total surface precipitation (Table 2). Despite the relatively low absolute rates, rain surface precipitation rates were found to be reduced with additional ship exhaust aerosol, agreeing with tendencies in ship exhaust cases to produce smaller r_e (Fig. 5c–d and Table 2). Changes in surface precipitation rates may significantly change with more-realistic ice formation parametrizations. As a result, we cannot exclude whether emissions associated with shipping activity may extend cloud lifetimes due to potential reductions in total precipitation rates (Albrecht, 1989).

In order to estimate the potential climatic impact of increased Arctic shipping activity, α, net short- (SW) and longwave (LW) radiative fluxes at the surface were characterized (Fig. 5e–f and Table 2). Net radiative fluxes were calculated by subtracting net upwelling fluxes from net downwelling

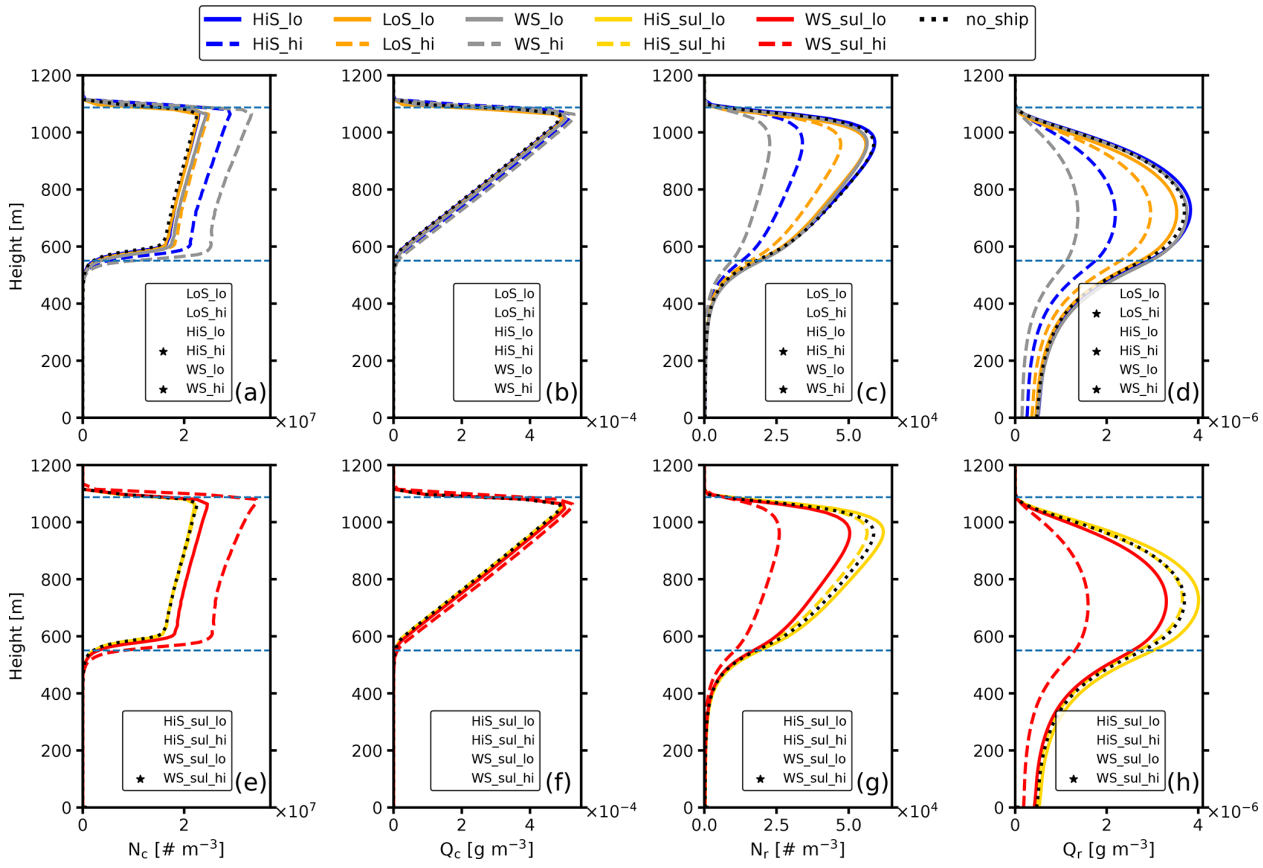

Figure 4. Vertical profiles of horizontally averaged **(a, e)** N_c, **(b, f)** Q_c, **(c, g)** N_r, and **(d, h)** Q_r averaged over the last 4 simulation hours. The dashed light-blue line represents the average cloud bottom and top height calculated for the reference case (no_ship). HiS, LoS, and WS represent ship aerosol from measurements of high- and low-sulfur-content fuels and wet scrubbing (Santos et al., 2022, 2023). The HiS_sul and WS_sul cases represent sulfate particle modes of high-FSC fuel combustion and exhaust gas wet scrubbing from Santos et al. (2024). The label additions _lo and _hi signify the ship aerosol concentrations used in the individual model runs. Significant differences between ship exhaust cases and no_ship were assessed using two-sided t tests at a confidence level of 95 %. Model runs with significant differences are marked by star icons in inset legends.

fluxes; hence, a negative value implies net outgoing radiation. At high latitudes, LW radiation generally has a larger influence on the surface energy budget compared to SW radiation, as solar radiation is limited outside the summer months. However, since the ASCOS case used in this study is based on observations from August, the net SW at the surface was also investigated.

With the exception of HiS_sul_hi, all ship sensitivity simulations tend to significantly increase α compared to no_ship (Fig. 5e–f). This observation agrees with the results shown in Figs. 4 and 5c–d, where tendencies towards generating larger N_c and reduced r_e values are shown. The largest increase in α is observed for WS_hi and WS_sul_hi, where cloud albedo increases from 0.65 to 0.70. The changes in LWP and r_e induced by ship aerosol perturbations are also seen in the LW net radiative fluxes at the surface (Fig. 5g–h).

Net LW fluxes at the surface are negative, meaning that the net radiative LW flux is upwelling and therefore cooling the surface. After about 5 h of simulation, net LW surface fluxes reach values of $\approx -13\,\mathrm{W\,m^{-2}}$ and eventually decrease to $\approx -15\,\mathrm{W\,m^{-2}}$ (no_ship) and $\approx -14.3\,\mathrm{W\,m^{-2}}$ (WS_hi) towards the end of the simulation. Ship cases, which are found to lead to the largest increase in LWP (HiS_hi, WS_hi, and WS_sul_hi; Fig. 2a–b), also reduce net LW cooling at the surface compared to no_ship; i.e., net LW becomes less negative. Our results suggest that ship exhaust perturbations may lead to diminished surface LW radiative cooling and could therefore lead to enhanced surface warming, that is, if the concentrations and size of the associated exhaust particle size distributions are sufficiently large to act as CCNs. Similar relationships between increased LWP and reduced LW radiative cooling were also noted by Christiansen et al. (2020).

The net SW radiation is positive in all simulations, meaning the net flux is downwelling. In all simulations, the net SW fluxes initially increase until 6 h into the respective simulations, where a maximum of around $14\,\mathrm{W\,m^{-2}}$ is reached. By

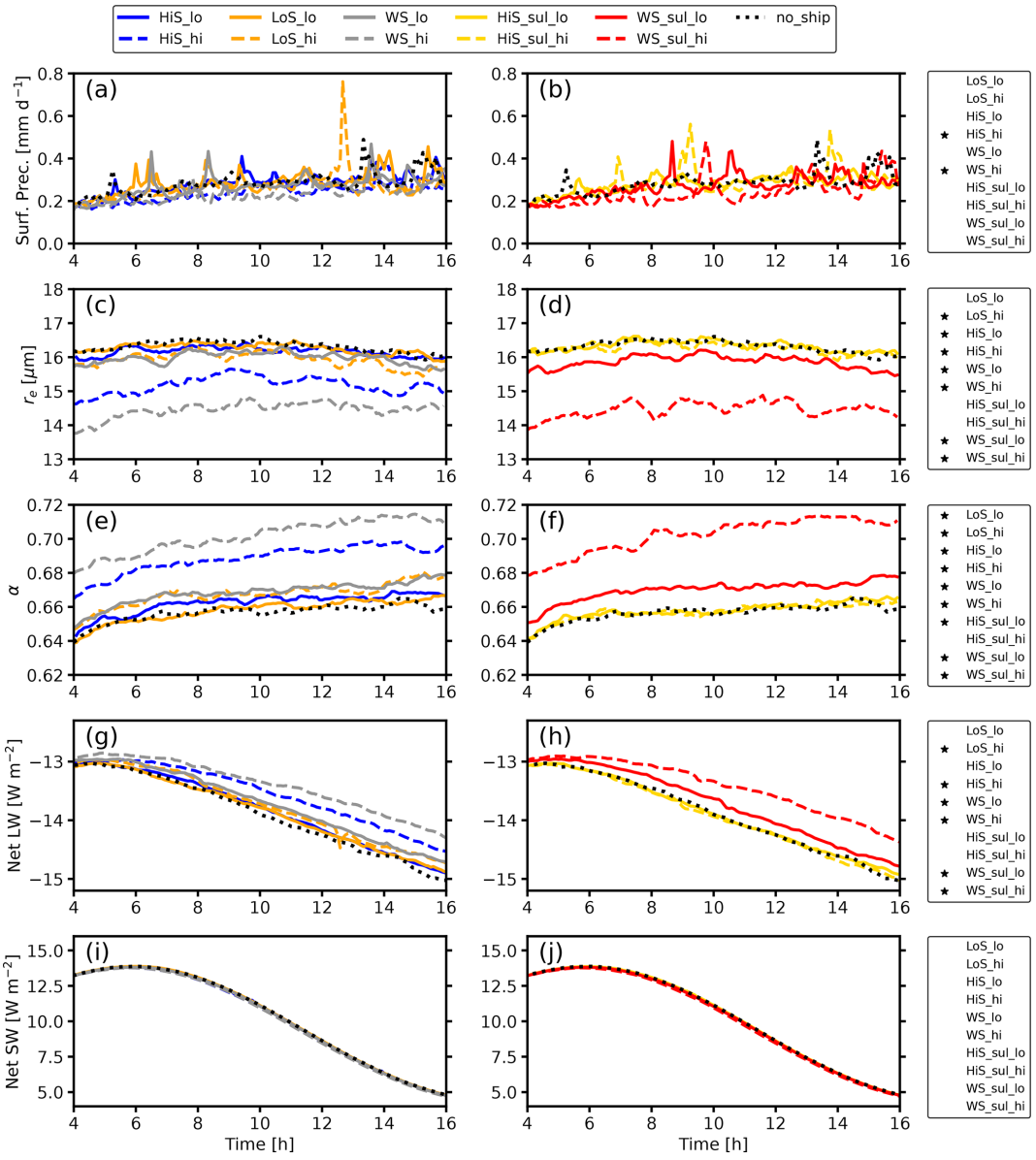

Figure 5. Time evolution of the simulated domain-averaged **(a, b)** surface precipitation, **(c, d)** r_e, **(e, f)** α, **(g, h)** net longwave radiation at the surface (net LW), and **(i, j)** net shortwave radiation at the surface (net SW) for the set of simulations. Net radiative fluxes are calculated by subtracting the upwelling radiative flux from the downwelling flux (e.g., $LW_{down} - LW_{up}$); hence, a negative value implies net outgoing radiation. no_ship refers to the reference case with background aerosol only. HiS, LoS, and WS represent ship aerosol from measurements of high- and low-sulfur-content fuels and wet scrubbing (Santos et al., 2022, 2023). The HiS_sul and WS_sul cases represent sulfate particle modes of high-FSC fuel combustion and exhaust gas wet scrubbing from Santos et al. (2024). The label additions _lo and _hi signify the ship aerosol concentrations used in the individual model runs. Significant differences between ship exhaust cases and no_ship were assessed using two-sided t tests at a confidence level of 95 %. Model runs with significant differences are marked by star icons in the right-hand-side legends. The last 4 simulation hours were used to perform statistical tests.

the end of the simulations, net SW decreases to $\approx 5\,W\,m^{-2}$. The temporal trends in LW and SW radiation both coincide with the solar angle. The results indicate that WS cases tend to slightly decrease the net SW (Table 2 and Fig. C1), yet none of the ship sensitivity tests were found to significantly impact net SW fluxes at the surface, despite associated increases in α (Fig. 5i–j). Changes in cloud properties induced by ship exhaust perturbations are expected to only lead to small changes in SW surface fluxes due to the reduced solar fluxes based on the geographical location and the comparatively large LWP, which leads to a substantial extinction of incoming SW radiation. Relatively small changes in α are

therefore only expected to lead to minor changes in SW surface fluxes.

3.4 Sensitivity to different levels of N_i

Additional simulations of no_ship, HiS_sul, and WS_sul were performed with N_i increased from 200 to 600 m^{-3}. The aim of these additional simulations was to investigate the susceptibility of a thinner mixed-phase cloud, i.e., with reduced LWP and cloud depth, to ship exhaust particle perturbations. When N_i is increased to 600 m^{-3}, the LWP is reduced by ≈ 45 % compared to no_ship and is close to the 75th percentile of the observational data (Fig. 6a). IWP is increased by 3.8 g m^{-2} (≈ 69 %; comparison between no_ship and no_ship_ni600) and is also within the observed range (Fig. 6b). With an increased N_i, ship exhaust particles do not lead to strong perturbations in LWP ($|\Delta LWP| < 3.2$ %) compared to sensitivity tests performed with $N_i = 200\ m^{-3}$. In fact, the ship exhaust sensitivity simulations display a tendency towards reducing the LWP compared to no_ship_ni600, which is in contrast to the model runs with $N_i = 200\ m^{-3}$ shown in Fig. 2. Such a muted response in LWP adjustments due to additional ship exhaust particles was also reported by Possner et al. (2017), who found a suppressed LWP response caused by ship-related CCN emissions when the number of ice nucleating particles was increased. The IWP, on the other hand, increased for no_ship_ni600, HiS_sul_hi_ni600, and WS_sul_hi_ni600 compared to no_ship (Fig. 6b), as all ice-phase hydrometeors increase substantially in number and mass concentrations (Fig. 7c–e and h–j). As with the first set of simulations, ship exhaust perturbations do not significantly impact the IWP compared to the respective reference case, no_ship_ni600, which, as previously discussed, is mainly due to the implementation of diagnostic N_i.

Figure 7 shows the impact on cloud depth and all hydrometeor classes for the _ni600 simulations compared to no_ship (with $N_i = 200\ m^{-3}$). The cloud depth is decreased, mostly due to adjustments in cloud bottom height, which increases by ≈ 80 m (Fig. 7). Taking into account the increase in cloud bottom height, N_c values are either similar (no_ship_ni600, HiS_sul_hi_ni600) or increased (WS_sul_hi_ni600), compared to the respective no_ship values (Fig. 7a). Simultaneously, Q_c values of all _ni600 cases are reduced compared to no_ship, suggesting smaller cloud droplets in the cloud (Fig. 7f). Raindrop number N_r and mass concentrations Q_r are significantly reduced compared to no_ship (Fig. 7b–g), resulting from reduced auto-conversion of cloud droplets to raindrops and droplet coalescence efficiency, as well as enhanced scavenging of raindrops by graupel and snow, which display substantial concentration increases in all _ni600 runs (Fig. 7d–e and i–j).

Surface precipitation rates are slightly increased in the _ni600 simulations compared to no_ship (< 10 %; Table 2 and Fig. 8a), which is due to enhancements in graupel formation (Fig. 7d and i). Liquid-phase surface precipitation rates are small and negligible for all _ni600 simulations. Average cloud drop effective radii r_e values are reduced by ≈ 1 µm compared to the respective simulations with $N_i = 200\ m^{-3}$, agreeing with observed reductions in LWP (Fig. 6a) and Q_c (Fig. 7f). The reductions in LWP and α are both reflected in the net radiative fluxes at the surface. Net LW radiative fluxes at the surface are reduced by at least 2 W m^{-2} compared to no_ship, meaning that reductions in LWP and cloud depth lead to reduced re-emission of LW radiation to the surface (Fig. 8d). Respective _ni600 ship exhaust cases tend to reduce net LW at the surface further, suggesting that in these instances ship exhaust perturbations would yield a slight net cooling effect. This is in contrast to the results shown in Sect. 3.3 where ship exhaust perturbations reduced net outgoing LW radiation at the surface. Relative reductions in α for _ni600 cases are reflected in net SW fluxes at the surface. In comparison to no_ship, net SW is on average increased by ≈ 0.5 W m^{-2} compared to no_ship (Fig. 8e and Table 2). Nevertheless, additional ship exhaust particles do not significantly alter net SW radiative surface fluxes (Fig. C2).

In summary, the results shown in this section demonstrate that the impact of ship exhaust particles on clouds and the surface radiative budget does not depend only on the ship exhaust particles themselves. The sensitivity is also strongly dependent on the background state of the atmosphere and the background cloud properties, such as cloud thickness. Interestingly, ship exhaust perturbations can have opposite effects on certain cloud parameters and net radiative fluxes. The most striking difference is that ship emissions tend to decrease the LWP and enhance net outgoing LW radiative surface fluxes when $N_i = 600\ m^{-3}$, whereas the opposite is true when $N_i = 200\ m^{-3}$.

4 Discussion

In general, ship emissions can lead to more but smaller liquid droplets in the mixed-phase clouds studied here. This means that even if the clouds contain more liquid water, rain surface precipitation is reduced. Nevertheless, this response was strongly coupled to the cloud IWP, which is an indicator of the cloud thickness. In our case study, total surface precipitation rates are dominated by graupel, which is not significantly affected by additional ship aerosol particles. Moreover, ship exhaust emissions have the potential to affect the cloud radiative processes that play a vital role in the Arctic climate system. While the shortwave radiative budget is mostly unaffected, ship exhaust perturbations can lead to both reductions and increases in net longwave radiative cooling at the surface and potentially impact the net surface radiative budget. The magnitude of the ship-exhaust-induced cloud perturbations is strongly dependent on the number concentrations of the particle emissions. It is also affected more by the size of the exhaust particles than by their hygroscopic-

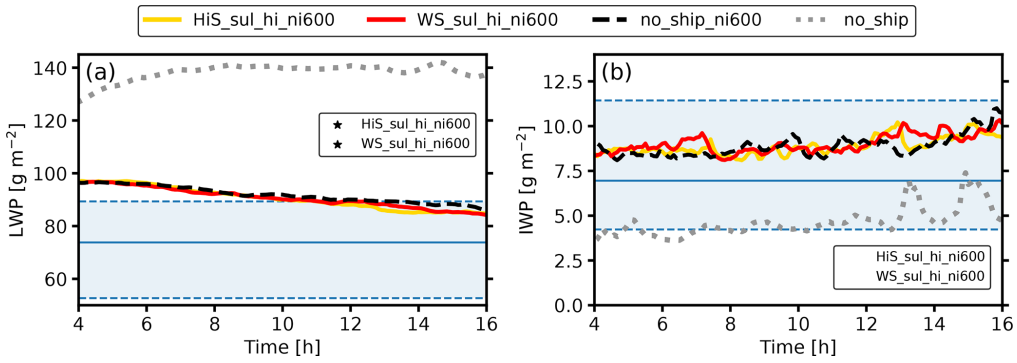

Figure 6. Time evolution of the simulated domain-averaged **(a)** liquid water path (LWP) and **(b)** ice water path (IWP). Panels show results for model runs where N_i was increased from 200 to 600 m^{-3}. Model runs with increased N_i are labeled with _ni600. The simulations are compared to the no_ship case where $N_i = 200\,\mathrm{m}^{-3}$. The blue-shaded area refers to the retrieved LWP and IWP from microwave radiometer measurements (the median over the observation period; the corresponding dashed lines are the 25th and 75th percentiles) during the ASCOS campaign (Tjernström et al., 2012, 2014). Only ship exhaust sensitivity cases with high concentrations (_hi) are shown in the figure. Significant differences between ship exhaust cases and no_ship_ni600 were assessed using two-sided t tests at a confidence level of 95 %. Model runs with significant differences are marked by star icons in inset legends. The last 4 simulation hours were used to perform statistical tests. The first 4 h are considered a spin-up period of the model and are removed from the panels.

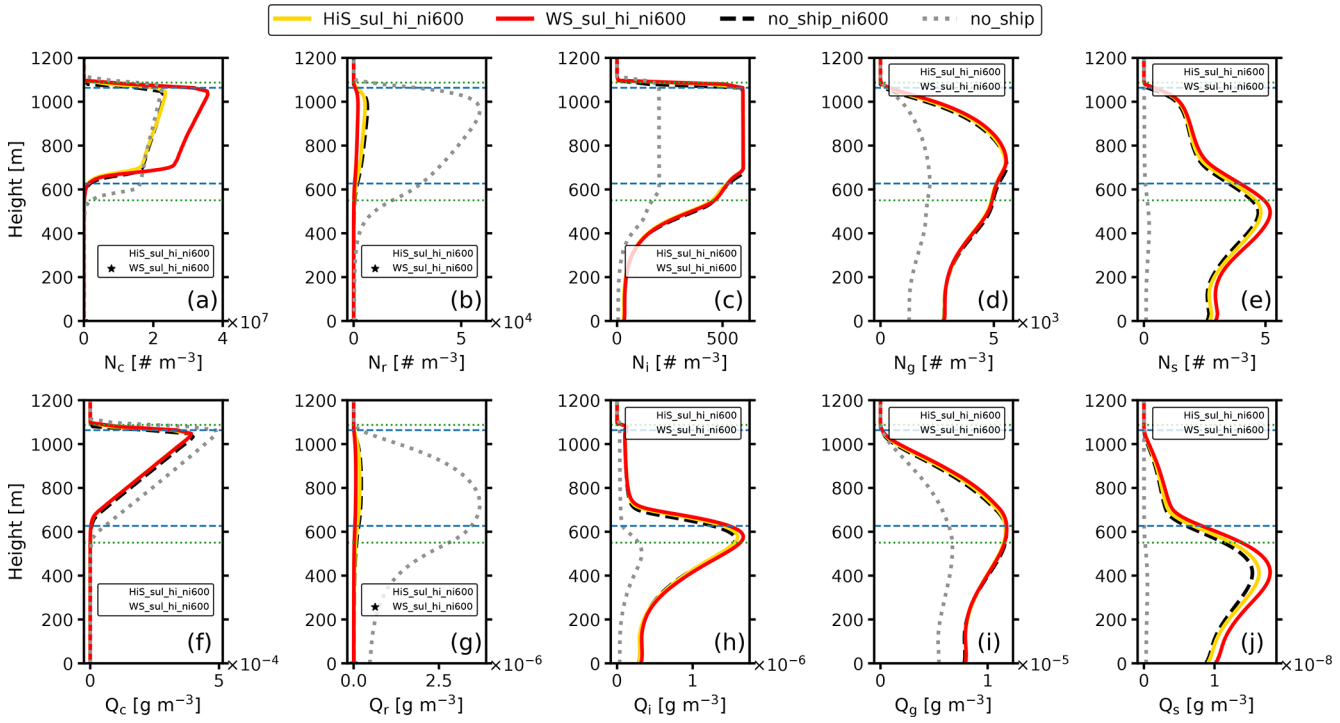

Figure 7. Vertical profiles of horizontally averaged **(a)** N_c, **(b)** N_r, **(c)** N_i, **(d)** N_g, **(e)** N_s, **(f)** Q_c, **(g)** Q_r, **(h)** Q_i, **(i)** Q_g, and **(j)** Q_s averaged over the last 4 simulation hours for no_ship_ni600, HiS_sul_hi_ni600, WS_sul_hi_ni600, and no_ship. The dashed light-blue line represents the average cloud bottom and cloud top heights calculated for no_ship_ni600 (dotted green line for no_ship). The HiS_sul and WS_sul cases represent sulfate particle modes of high-FSC fuel combustion and exhaust gas wet scrubbing. Significant differences between ship exhaust cases and no_ship_ni600 were assessed using two-sided t tests at a confidence level of 95 %. Model runs with significant differences are marked by star icons in inset legends.

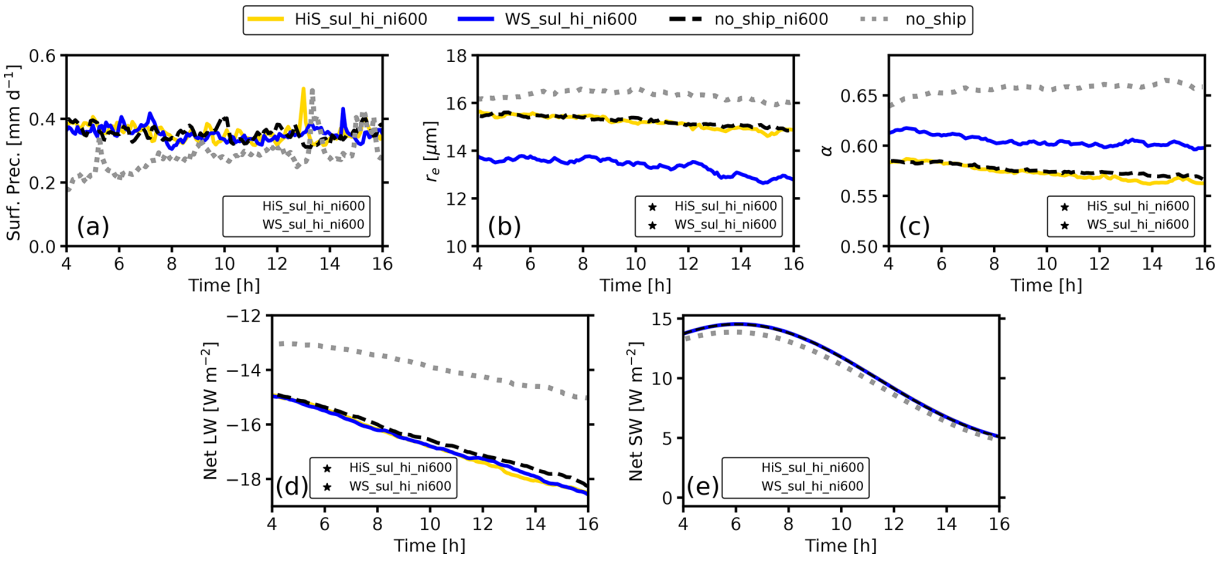

Figure 8. Time evolution of the simulated domain-averaged **(a)** surface precipitation rates, **(b)** r_e, **(c)** α, **(d)** net longwave radiation at the surface (net LW), and **(e)** net shortwave radiation at the surface (net SW) for a set of simulations with $N_i = 600\,m^{-3}$ (_ni600) and the no_ship case ($N_i = 200\,m^{-3}$). Net radiative fluxes are calculated by subtracting the upwelling radiative flux from the downwelling flux (e.g., $LW_{down} - LW_{up}$); hence, a negative value implies net outgoing radiation. no_ship refers to the reference case with background aerosol only. The HiS_sul and WS_sul cases represent sulfate particle modes of high-FSC fuel combustion and exhaust gas wet scrubbing from Santos et al. (2024). Only ship exhaust sensitivity cases with high concentrations (_hi) are shown in the figure. Significant differences between ship exhaust cases and no_ship_ni600 were assessed using two-sided t tests at a confidence level of 95 %. Model runs with significant differences are marked by star icons in inset legends. The last 4 simulation hours were used to perform statistical tests.

ity. This means that the impact of ship emissions on Arctic cloud properties would depend strongly on the fuel types used and whether exhaust aftertreatment systems like scrubbers are used. Uncertainties in Arctic fuel type projections increase the challenge of constraining regional climate impacts from Arctic shipping. Transitions towards fuels with reduced sulfur content have been shown to lead to substantial reductions in CCN number emissions, which potentially could reduce radiative effects from ship aerosol–cloud interactions. This is due to a reduction in hygroscopicity of the ship exhaust particles (Santos et al., 2023, 2024) and a shift in the particle size distribution towards smaller sizes (decreasing CMD; Lack et al., 2011; Yu et al., 2020, 2023). From June 2025, ships will no longer be allowed to carry and use fuel oils with densities and viscosities exceeding predefined limits (IMO, 2021), which could have ramifications for wet-scrubber usage, as these systems are mainly designed for use with high-FSC-residual fuels. Moreover, due to environmental concerns associated with increased Arctic shipping activity, Canada and several organizations have proposed BC emission control areas for Arctic waters that include mandates for low-FSC distillate fuel usage for ships operating in the Arctic (IMO, 2023b, a). Assuming that these proposals are ratified, they would limit the allowed Arctic ship fuels and thus facilitate estimating the climate impact from shipping. In this case, other environmental impacts from shipping such as BC deposition on snow surfaces, which reduces the surface albedo and enhances surface warming, could play a larger role and dominate the climate impact from Arctic shipping.

Ship exhaust particle concentrations above $1000\,cm^{-3}$ are realistic if one considers narrower and more-localized regions where ship exhaust particles perturb clouds (Hobbs et al., 2000; Possner et al., 2018). Once emitted by a transiting ship, exhaust particles become dispersed in the atmosphere, generally resulting in smaller particle number concentrations. As a result, perturbations would likely cause changes in cloud properties more akin to our low-concentration model runs. One area of focus for future research could be implementing ship plume dispersion and using more-realistic vertical exhaust particle concentration profiles. Moreover, exhaust particles will undergo chemical and physical transformations in the atmosphere associated with ship exhaust plume aging. In aged plumes, changes in particle size distributions are often observed due to coagulation of exhaust particles and condensation and evaporation of water vapor and other atmospheric substances (Petzold et al., 2008; Celik et al., 2020). If, for example, fewer but larger particles are present, it could have a stronger impact on cloud hydrometeors compared to the ship exhaust particle size distributions and number concentrations implemented in this study.

While this study focuses on Arctic shipping and clouds, IMO FSC regulations apply worldwide. This means that global ship exhaust emissions are subject to changes and thus

the global radiative forcing exerted by ship exhaust emissions will likely change. It is therefore important to improve our general understanding of the potential effects of FSC reduction and wet scrubbing on particulate matter emissions and what this implies for cloud and climate processes.

5 Conclusions

In this study, we used LES together with aerosol data from laboratory experiments to examine the potential impact of ship exhaust particles on Arctic mixed-phase cloud properties. The laboratory experiments investigated the impacts of fuel sulfur content reduction and exhaust wet scrubbing on the physicochemical properties of ship exhaust particles (Santos et al., 2022, 2023, 2024). Wet scrubbing and FSC reduction represent regulatory compliance measures in the maritime shipping sector, which affect ship exhaust particle emissions and could potentially be utilized by ships in the Arctic. Given the projected increase in Arctic shipping activity due to strongly declining Arctic sea-ice extent and the availability of shorter trans-Arctic transportation routes, we have sought to illuminate how ship emissions may impact Arctic clouds and thereby affect the regional radiative balance.

The simulations were done for a persistent stratiform mixed-phase cloud based on observations from the ASCOS campaign (Tjernström et al., 2012, 2014) and on previous simulations (Igel et al., 2017; Stevens et al., 2018; Christiansen et al., 2020; Sotiropoulou et al., 2021; Frostenberg et al., 2023). The simulated cloud was subsequently perturbed by adding ship exhaust particle profiles into the model domain. A selected number of model runs were repeated with increased pre-fixed N_i to study the impact of ship exhaust perturbations on a thinner baseline cloud with an increased IWP and reduced LWP.

Ship exhaust simulations revealed potential impacts on cloud droplet and raindrop concentrations, affecting the LWP and decreasing the cloud drop effective radius. Total surface precipitation was found to be mostly unaffected; liquid-phase precipitation was reduced, but it was only a minor constituent of total surface precipitation. Moreover, the cloud albedo increased marginally in all ship exhaust experiments. Our first set of simulations, with N_i concentrations in line with observations and IWP values at the lower end of the retrieved values, demonstrated that ship exhaust perturbations can lead to a reduction in longwave radiative cooling of up to $0.7\,W\,m^{-2}$ at the surface. This result implies that ship emissions may lead to a net warming effect compared to our baseline simulation without ship exhaust aerosol. The magnitude of the surface radiation change depended on the hygroscopicity and the CMD of the added ship aerosol particles, where the effect of the CMD was most important. Additional sensitivity tests with N_i increased to $600\,m^{-3}$ and with a reduced LWP and increased IWP (both in line with retrieved values) revealed that ship exhaust perturbations may lead to enhanced surface radiative cooling. This demonstrates that the net effect of ship exhaust emissions on the radiative forcing exerted by Arctic low-level clouds strongly depends on not only the prevalent fuel types and whether ships in the Arctic utilize wet scrubbers for exhaust aftertreatment but also the prevalent atmospheric conditions and cloud properties. Studies have shown that Arctic low-level-cloud properties are strongly coupled to the surface properties and that sea-ice-free conditions can lead to generally larger cloud fractions and an increased LWP (Barton and Veron, 2012; Taylor and Monroe, 2023). It is therefore likely that future Arctic low-level-cloud properties may be more similar to our first case ($N_i = 200\,m^{-2}$).

Bulatovic et al. (2021) showed large variations in cloud microphysical properties for different background aerosol concentrations and sizes. Results of ship exhaust perturbations may therefore vary substantially with different background aerosol concentrations and thus the microphysical structure of the perturbed cloud, as demonstrated by our additional set of simulations with increased N_i. Consequently, it is important to highlight that the case study used in this study is based on observations made in the high Arctic. Most Arctic shipping activity will likely occur closer to coastal regions, where air masses are likely to be more strongly influenced by anthropogenic and biogenic activity (see, for example, Smith and Stephenson, 2013). This means that the atmospheric background conditions and cloud properties may vary from the mixed-phase cloud case studied here and will likely affect the impact of ship exhaust perturbations on cloud properties. Moreover, the enhanced warming that the Arctic is experiencing will likely change the state of ambient aerosol concentrations due to biogenic and anthropogenic processes (Schmale et al., 2021). For example, more open sea surface area will lead to enhanced new-particle formation due to marine biogenic emissions (Dall'Osto et al., 2017). General low ambient aerosol number concentrations mean that already small increases in concentrations can have large impacts on cloud properties (Mauritsen et al., 2011). It is therefore expected that these changes will also affect the properties of Arctic clouds.

Our collective results do show evidence that Arctic shipping emissions can lead to alterations in the micro- and macrophysical state of persistent Arctic low-level mixed-phase clouds. While a stronger tendency towards enhanced surface warming from ship exhaust emissions was noted, this effect was mostly observed when ship aerosol concentrations were increased by $N = 1000\,cm^{-3}$. When low ship exhaust particle concentrations ($N = 100\,cm^{-3}$) were utilized, only wet-scrubbing model runs were found to alter cloud radiative properties significantly compared to the baseline. However, given the ban on carriage and usage of high-density/viscosity residual fuel oils in 2025, wet scrubbing might not be utilized by a large fraction of ships in the Arctic (IMO, 2021).

This study may help to constrain possible climate feedbacks from a projected increase in Arctic shipping activity.

However, our results show that more information on future Arctic shipping activity, including fuel types, traffic volume and associated emissions characteristics, prevalent meteorological conditions, and cloud types, is required for more accurate estimates.

Appendix A: Meteorological parameters of the ASCOS case

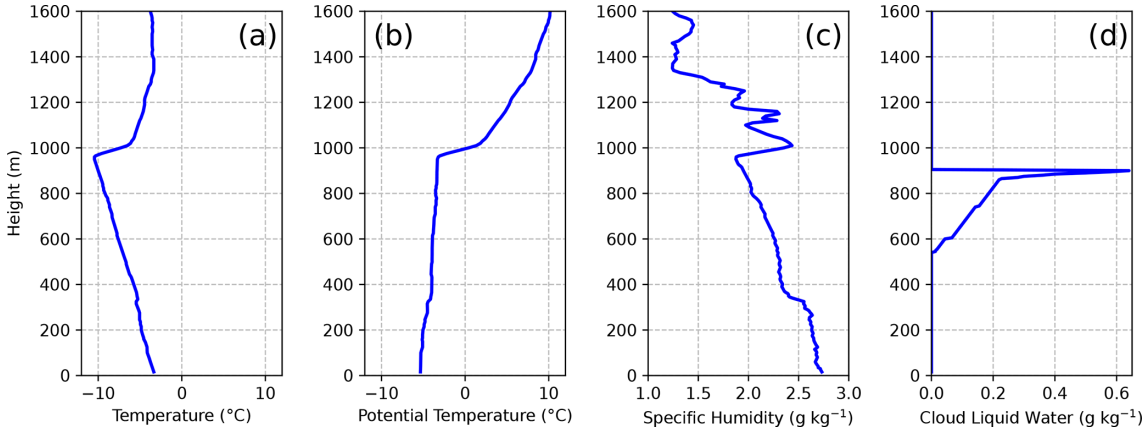

Figure A1. Radiosonde observations of **(a)** temperature, **(b)** potential temperature, **(c)** specific humidity, and **(d)** derived cloud liquid water based on radiometer measurements performed on 31 August 2008 during the ASCOS campaign (Tjernström et al., 2012, 2014). The data were used to initialize MIMICA in this study.

Appendix B: Profiles of ice-phase hydrometeors

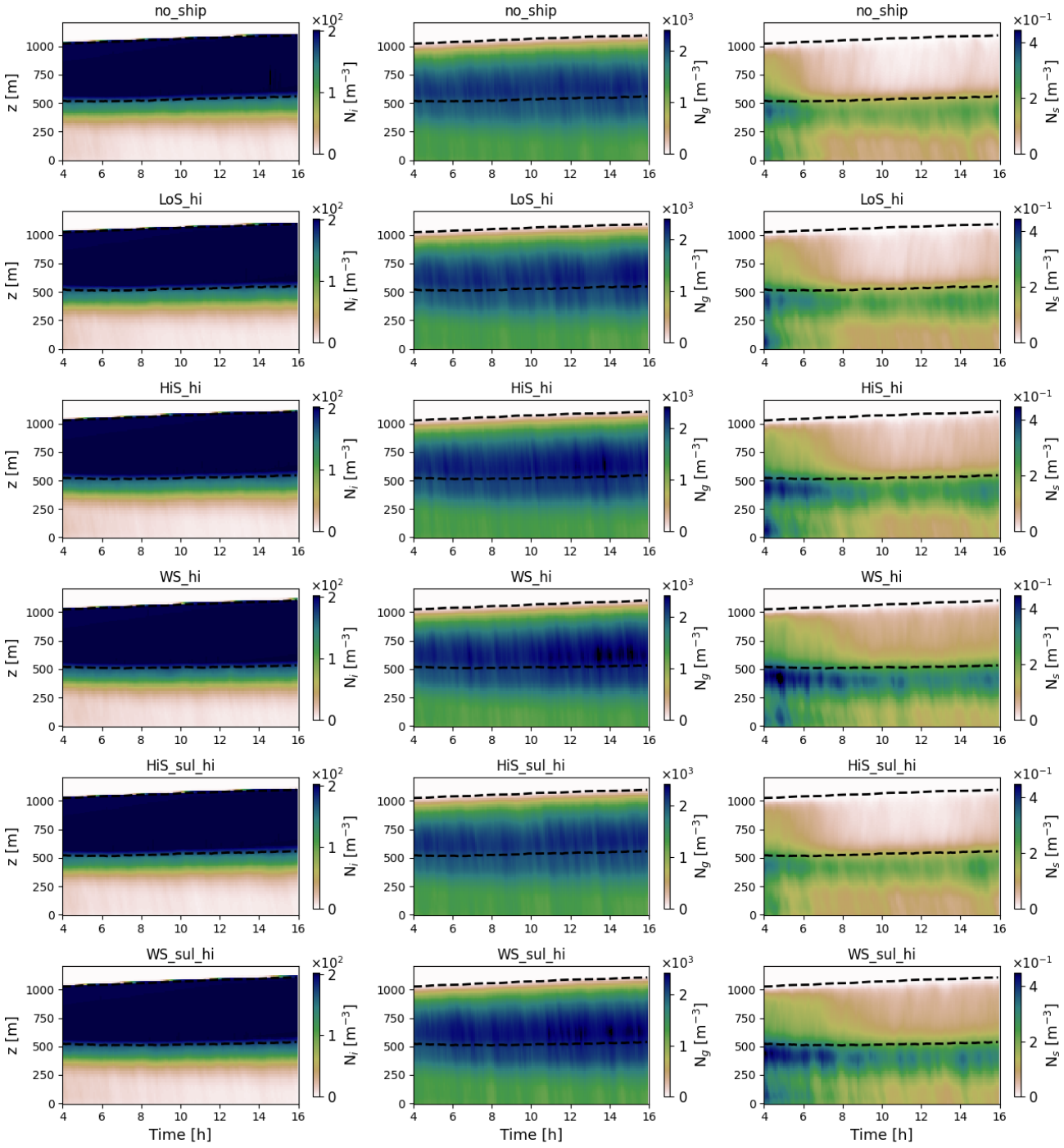

Figure B1. Temporal evolution of horizontally averaged number concentrations of ice crystals (N_i), graupel (N_g), and snow (N_s) simulated for the reference case (no_ship) and the high ship aerosol concentration cases (LoS_hi, HiS_hi, WS_hi, HiS_sul_hi, and WS_sul_hi). The dashed black lines represent case-specific horizontally averaged cloud bottom and cloud top heights. The spin-up period (0 to 4 h) is removed from all panels.

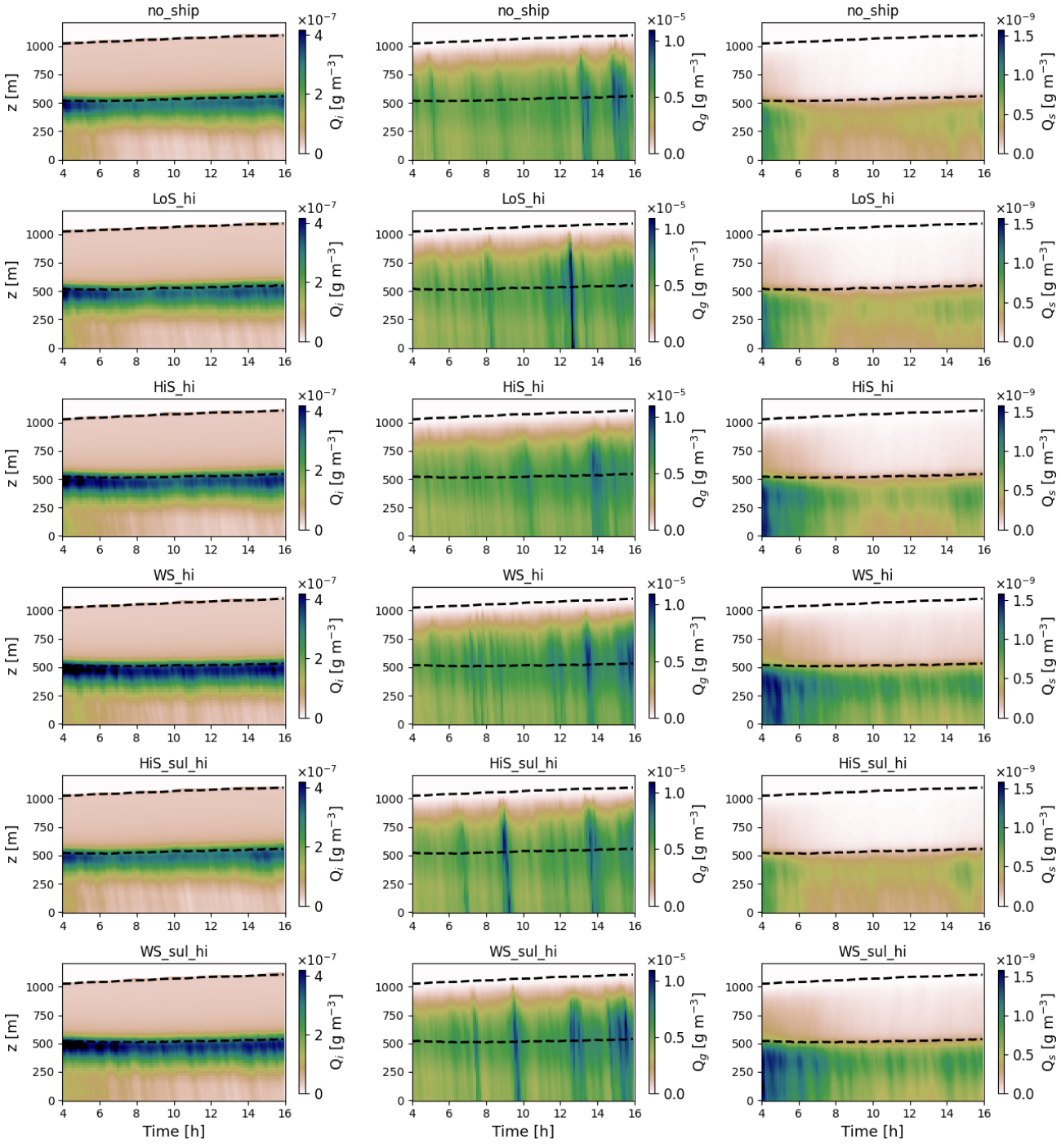

Figure B2. Temporal evolution of horizontally averaged mixing ratios of ice crystals (Q_i), graupel (Q_g), and snow (Q_s) simulated for the reference case (no_ship) and the high ship aerosol concentration cases (LoS_hi, HiS_hi, WS_hi, HiS_sul_hi, and WS_sul_hi). The dashed black lines represent case-specific horizontally averaged cloud bottom and cloud top heights. The spin-up period (0 to 4 h) is removed from all panels.

Appendix C: Net shortwave surface fluxes

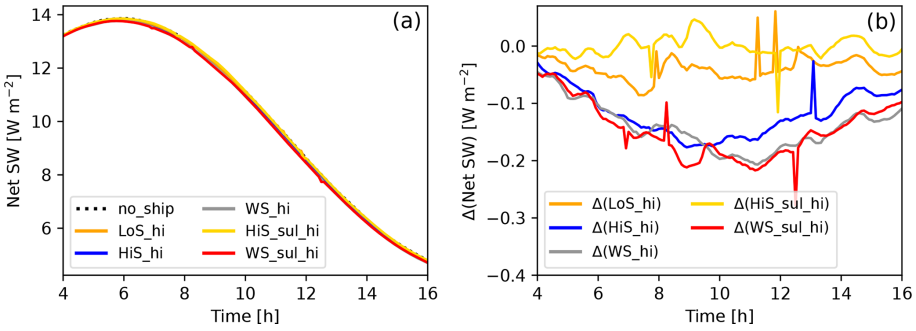

Figure C1. **(a)** Time evolution of the simulated domain-averaged net shortwave radiation at the surface (net SW) for the set of ship exhaust sensitivity cases with $N_i = 200\,m^{-3}$ and the corresponding no_ship case. Only ship exhaust sensitivity cases with high concentrations (_hi) are shown in the figure. **(b)** Corresponding absolute changes in net SW surface fluxes calculated as $(\text{net SW})_{\text{ship}} - (\text{net SW})_{\text{no\_ship}}$.

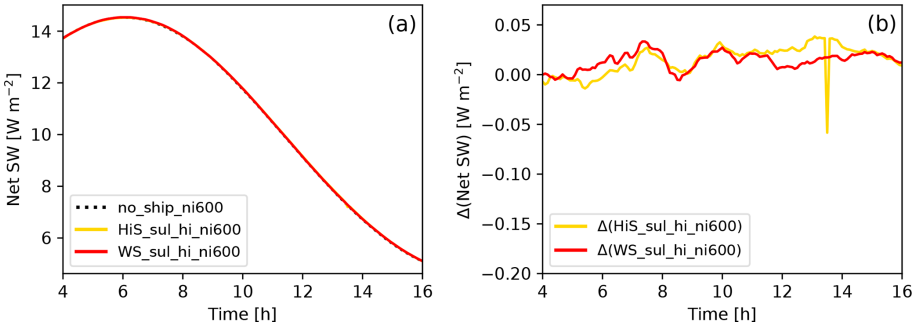

Figure C2. **(a)** Time evolution of the simulated domain-averaged net shortwave radiation at the surface (net SW) for the set of ship exhaust sensitivity cases with $N_i = 600\,m^{-3}$ and the corresponding no_ship_ni600 case. Only ship exhaust sensitivity cases with high concentrations (_hi) are shown in the figure. **(b)** Corresponding absolute changes in net SW surface fluxes calculated as $(\text{net SW})_{\text{ship}} - (\text{net SW})_{\text{no\_ship}}$.

Appendix D: Averaged profiles of ice-phase hydrometeors

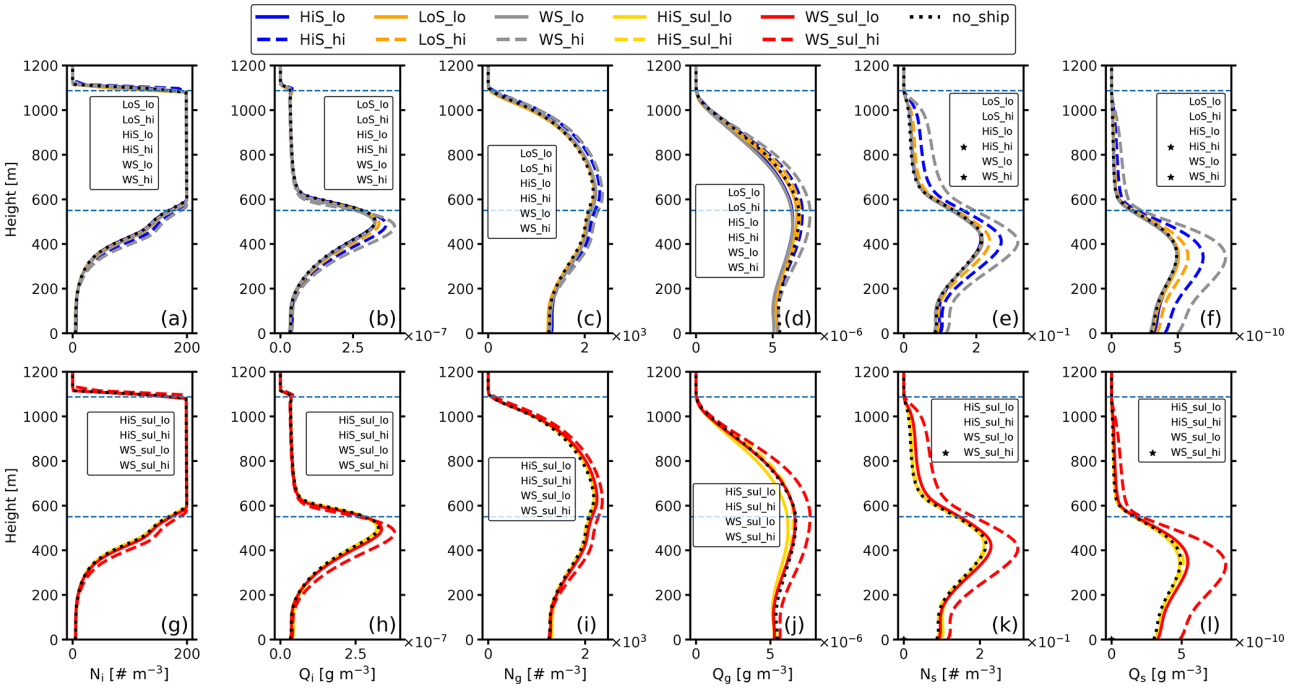

Figure D1. Vertical profiles of horizontally averaged **(a, g)** N_i, **(b, h)** Q_i, **(c, i)** N_g, **(d, j)** Q_g, **(e, k)** N_s, and **(f, l)** Q_s averaged over the last 4 simulation hours. The dashed light-blue line represents the average cloud bottom and cloud top heights calculated for the reference case (no_ship). HiS, LoS, and WS represent ship aerosol from measurements of high- and low-sulfur-content fuels and wet scrubbing (Santos et al., 2022, 2023). The HiS_sul and WS_sul cases represent sulfate particle modes of high-FSC fuel combustion and exhaust gas wet scrubbing from Santos et al. (2024). The label additions _lo and _hi signify the ship aerosol concentrations used in the individual model runs. Significant differences between ship exhaust cases and no_ship were assessed using two-sided t tests at a confidence level of 95 %. Model runs with significant differences are marked by star icons in inset legends.

Data availability. The model output data presented in this study are available at https://doi.org/10.5281/zenodo.12166747 (Escusa dos Santos et al., 2024). The experimental data utilized in this study have been previously published and are made available through the cited publications (Santos et al., 2022, 2023, 2024).

Author contributions. Idea – EST and AMLE. Conceptualization – LI, HCF, and AMLE. Model implementation and simulations – LFEdS, HCF, LI, and ABP. Analysis of the data – LFEdS, HCF, LI, and ABP. Visualization – LFEdS. Writing, review, and editing – all co-authors.

Competing interests. The contact author has declared that none of the authors has any competing interests.

Disclaimer. Publisher's note: Copernicus Publications remains neutral with regard to jurisdictional claims made in the text, published maps, institutional affiliations, or any other geographical representation in this paper. While Copernicus Publications makes every effort to include appropriate place names, the final responsibility lies with the authors.

Acknowledgements. The research presented in this paper is a contribution to the Strategic Research Area "ModElling the Regional and Global Earth system", MERGE, funded by the Swedish government.

Financial support. This research has been supported by the Swedish Research Councils Formas (grant no. 2017-00564) and Vetenskapsrådet (grant nos. 2020-03497 and 2020-04158). Hannah C. Frostenberg and Luisa Ickes were supported by the Chalmers Gender Initiative for Excellence (Genie). Alejandro Baró Pérez was supported by MERGE. The computations were enabled by resources provided by the National Academic Infrastructure for Supercomputing in Sweden (NAISS) at the National Supercomputer Centre (NSC), partially funded by the Swedish Research Council Vetenskapsrådet (grant agreement no. 2022-06725).

The publication of this article was funded by the Swedish Research Council, Forte, Formas, and Vinnova.

Review statement. This paper was edited by Matthew Lebsock and reviewed by two anonymous referees.

References

Albrecht, B. A.: Aerosols, Cloud Microphysics, and Fractional Cloudiness, Science, 245, 1227–1230, https://doi.org/10.1126/science.245.4923.1227, 1989.

Andreasen, A. and Mayer, S.: Use of seawater scrubbing for SO2 removal from marine engine exhaust gas, Energ. Fuel., 21, 3274–3279, https://doi.org/10.1021/ef700359w, 2007.

Barton, N. and Veron, D.: Response of clouds and surface energy fluxes to changes in sea-ice cover over the Laptev Sea (Arctic Ocean), Clim. Res., 54, 69–84, https://doi.org/10.3354/cr01101, 2012.

Browse, J., Carslaw, K. S., Schmidt, A., and Corbett, J. J.: Impact of future Arctic shipping on high-latitude black carbon deposition, Geophys. Res. Lett., 40, 4459–4463, https://doi.org/10.1002/grl.50876, 2013.

Bulatovic, I., Igel, A. L., Leck, C., Heintzenberg, J., Riipinen, I., and Ekman, A. M. L.: The importance of Aitken mode aerosol particles for cloud sustenance in the summertime high Arctic – a simulation study supported by observational data, Atmos. Chem. Phys., 21, 3871–3897, https://doi.org/10.5194/acp-21-3871-2021, 2021.

Bulatovic, I., Savre, J., Tjernström, M., Leck, C., and Ekman, A. M. L.: Large-eddy simulation of a two-layer boundary-layer cloud system from the Arctic Ocean 2018 expedition, Atmos. Chem. Phys., 23, 7033–7055, https://doi.org/10.5194/acp-23-7033-2023, 2023.

Celik, S., Drewnick, F., Fachinger, F., Brooks, J., Darbyshire, E., Coe, H., Paris, J.-D., Eger, P. G., Schuladen, J., Tadic, I., Friedrich, N., Dienhart, D., Hottmann, B., Fischer, H., Crowley, J. N., Harder, H., and Borrmann, S.: Influence of vessel characteristics and atmospheric processes on the gas and particle phase of ship emission plumes: in situ measurements in the Mediterranean Sea and around the Arabian Peninsula, Atmos. Chem. Phys., 20, 4713–4734, https://doi.org/10.5194/acp-20-4713-2020, 2020.

Christensen, M. W., Suzuki, K., Zambri, B., and Stephens, G. L.: Ship track observations of a reduced shortwave aerosol indirect effect in mixed-phase clouds, Geophys. Res. Lett., 41, 6970–6977, https://doi.org/10.1002/2014GL061320, 2014.

Christiansen, S., Ickes, L., Bulatovic, I., Leck, C., Murray, B. J., Bertram, A. K., Wagner, R., Gorokhova, E., Salter, M. E., Ekman, A. M., and Bilde, M.: Influence of Arctic Microlayers and Algal Cultures on Sea Spray Hygroscopicity and the Possible Implications for Mixed-Phase Clouds, J. Geophys. Res.-Atmos., 125, e2020JD032808, https://doi.org/10.1029/2020JD032808, 2020.

Coakley, J. A., Bernstein, R. L., and Durkee, P. A.: Effect of Ship-Stack Effluents on Cloud Reflectivity, Science, 237, 1020–1022, https://doi.org/10.1126/science.237.4818.1020, 1987.

Corbett, J. J., Winebrake, J. J., Green, E. H., Kasibhatla, P., Eyring, V., and Lauer, A.: Mortality from Ship Emissions: A Global Assessment, Environ. Sci. Technol., 41, 8512–8518, https://doi.org/10.1021/es071686z, 2007.

Corbett, J. J., Lack, D. A., Winebrake, J. J., Harder, S., Silberman, J. A., and Gold, M.: Arctic shipping emissions inventories and future scenarios, Atmos. Chem. Phys., 10, 9689–9704, https://doi.org/10.5194/acp-10-9689-2010, 2010.

Dall'Osto, M., Beddows, D. C. S., Tunved, P., Krejci, R., Ström, J., Hansson, H.-C., Yoon, Y. J., Park, K.-T., Becagli, S., Udisti, R., Onasch, T., O'Dowd, C. D., Simó, R., and Harrison, R. M.: Arctic sea ice melt leads to atmospheric new particle formation, Sci. Rep., 7, 3318, https://doi.org/10.1038/s41598-017-03328-1, 2017.

Dalsøren, S. B., Samset, B. H., Myhre, G., Corbett, J. J., Minjares, R., Lack, D., and Fuglestvedt, J. S.: Environmental impacts of shipping in 2030 with a particular focus on the Arctic region, Atmos. Chem. Phys., 13, 1941–1955, https://doi.org/10.5194/acp-13-1941-2013, 2013.

Durkee, P. A., Noone, K. J., Ferek, R. J., Johnson, D. W., Taylor, J. P., Garrett, T. J., Hobbs, P. V., Hudson, J. G., Bretherton, C. S., Innis, G., Frick, G. M., Hoppel, W. A., O'Dowd, C. D., Russell, L. M., Gasparovic, R., Nielsen, K. E., Tessmer, S. A., Öström, E., Osborne, S. R., Flagan, R. C., Seinfeld, J. H., and Rand, H.: The Impact of Ship-Produced Aerosols on the Microstructure and Albedo of Warm Marine Stratocumulus Clouds: A Test of MAST Hypotheses 1i and 1ii, J. Atmos. Sci., 57, 2554–2569, https://doi.org/10.1175/1520-0469(2000)057<2554:TIOSPA>2.0.CO;2, 2000.

Eirund, G. K., Possner, A., and Lohmann, U.: Response of Arctic mixed-phase clouds to aerosol perturbations under different surface forcings, Atmos. Chem. Phys., 19, 9847–9864, https://doi.org/10.5194/acp-19-9847-2019, 2019.

Escusa dos Santos, L. F., Frostenberg, H., Baró Pérez, A., Ekman, A. M. L., Ickes, L., and Thomson, E. S.: Model output from "Potential impacts of marine fuel regulations on an Arctic stratocumulus case and its radiative response", Zenodo [data set], https://doi.org/10.5281/zenodo.12166747, 2024.

Eyring, V., Isaksen, I. S., Berntsen, T., Collins, W. J., Corbett, J. J., Endresen, O., Grainger, R. G., Moldanova, J., Schlager, H., and Stevenson, D. S.: Transport impacts on atmosphere and climate: Shipping, Atmos. Environ., 44, 4735–4771, https://doi.org/10.1016/j.atmosenv.2009.04.059, 2010.

Freud, E. and Rosenfeld, D.: Linear relation between convective cloud drop number concentration and depth for rain initiation, J. Geophys. Res.-Atmos., 117, D02207, https://doi.org/10.1029/2011JD016457, 2012.

Fridell, E. and Salo, K.: Measurements of abatement of particles and exhaust gases in a marine gas scrubber, P. I. Mech. Eng. M-J. Eng., 230, 154–162, https://doi.org/10.1177/1475090214543716, 2016.

Frostenberg, H. C., Welti, A., Luhr, M., Savre, J., Thomson, E. S., and Ickes, L.: The chance of freezing – a conceptional study to parameterize temperature-dependent freezing by including randomness of ice-nucleating particle concentrations, Atmos. Chem. Phys., 23, 10883–10900, https://doi.org/10.5194/acp-23-10883-2023, 2023.

Fu, Q. and Liou, K. N.: On the Correlated k-Distribution Method for Radiative Transfer in Nonhomogeneous Atmospheres, J. Atmos. Sci., 49, 2139–2156, https://doi.org/10.1175/1520-0469(1992)049<2139:OTCDMF>2.0.CO;2, 1992.

Gilgen, A., Huang, W. T. K., Ickes, L., Neubauer, D., and Lohmann, U.: How important are future marine and shipping aerosol emissions in a warming Arctic summer and autumn?, Atmos. Chem.

Phys., 18, 10521–10555, https://doi.org/10.5194/acp-18-10521-2018, 2018.

Gryspeerdt, E., Smith, T. W. P., O'Keeffe, E., Christensen, M. W., and Goldsworth, F. W.: The Impact of Ship Emission Controls Recorded by Cloud Properties, Geophys. Res. Lett., 46, 12547–12555, https://doi.org/10.1029/2019GL084700, 2019.

Hobbs, P. V., Garrett, T. J., Ferek, R. J., Strader, S. R., Hegg, D. A., Frick, G. M., Hoppel, W. A., Gasparovic, R. F., Russell, L. M., Johnson, D. W., O'Dowd, C., Durkee, P. A., Nielsen, K. E., and Innis, G.: Emissions from ships with respect to their effects on clouds, J. Atmos. Sci., 57, 2570–2590, https://doi.org/10.1175/1520-0469(2000)057<2570:EFSWRT>2.0.CO;2, 2000.

Igel, A. L., Ekman, A. M. L., Leck, C., Tjernström, M., Savre, J., and Sedlar, J.: The free troposphere as a potential source of arctic boundary layer aerosol particles, Geophys. Res. Lett., 44, 7053–7060, https://doi.org/10.1002/2017GL073808, 2017.

IMO: RESOLUTION MEPC.176(58) – Revised MARPOL Annex VI, International Maritime Organization (IMO), 2008.

IMO: RESOLUTION MEPC.329(76) – Prohibition on the use and carriage for use as fuel of heavy fuel oil by ships in Arctic waters, International Maritime Organization (IMO), 2021.

IMO: MEPC 80/9/1 – Reducing Black Carbon emissions in the Arctic, International Maritime Organization (IMO), 2023a.

IMO: MEPC 80/16/2 – Development of a proposal to designate a Canadian Arctic Emission Control Area, International Maritime Organization (IMO), 2023b.

Intrieri, J. M., Fairall, C. W., Shupe, M. D., Persson, P. O. G., Andreas, E. L., Guest, P. S., and Moritz, R. E.: An annual cycle of Arctic surface cloud forcing at SHEBA, J. Geophys. Res.-Oceans, 107, SHE 13-1–SHE 13-14, https://doi.org/10.1029/2000JC000439, 2002.

Jeong, S., Bendl, J., Saraji-Bozorgzad, M., Käfer, U., Etzien, U., Schade, J., Bauer, M., Jakobi, G., Orasche, J., Fisch, K., Cwierz, P. P., Rüger, C. P., Czech, H., Karg, E., Heyen, G., Krausnick, M., Geissler, A., Geipel, C., Streibel, T., Schnelle-Kreis, J., Sklorz, M., Schulz-Bull, D. E., Buchholz, B., Adam, T., and Zimmermann, R.: Aerosol emissions from a marine diesel engine running on different fuels and effects of exhaust gas cleaning measures, Environ. Pollut., 316, 120526, https://doi.org/10.1016/j.envpol.2022.120526, 2023.

Jonson, J. E., Gauss, M., Schulz, M., Jalkanen, J.-P., and Fagerli, H.: Effects of global ship emissions on European air pollution levels, Atmos. Chem. Phys., 20, 11399–11422, https://doi.org/10.5194/acp-20-11399-2020, 2020.

Kanji, Z. A., Welti, A., Corbin, J. C., and Mensah, A. A.: Black Carbon Particles Do Not Matter for Immersion Mode Ice Nucleation, Geophys. Res. Lett., 47, 1–9, https://doi.org/10.1029/2019GL086764, 2020.

Kuittinen, N., Jalkanen, J.-P., Alanen, J., Ntziachristos, L., Hannuniemi, H., Johansson, L., Karjalainen, P., Saukko, E., Isotalo, M., Aakko-Saksa, P., Lehtoranta, K., Keskinen, J., Simonen, P., Saarikoski, S., Asmi, E., Laurila, T., Hillamo, R., Mylläri, F., Lihavainen, H., Timonen, H., and Rönkkö, T.: Shipping Remains a Globally Significant Source of Anthropogenic PN Emissions Even after 2020 Sulfur Regulation, Environ. Sci. Technol., 55, 129–138, https://doi.org/10.1021/acs.est.0c03627, 2021.

Kupiszewski, P., Leck, C., Tjernström, M., Sjogren, S., Sedlar, J., Graus, M., Müller, M., Brooks, B., Swietlicki, E., Norris, S., and Hansel, A.: Vertical profiling of aerosol particles and trace gases over the central Arctic Ocean during summer, Atmos. Chem. Phys., 13, 12405–12431, https://doi.org/10.5194/acp-13-12405-2013, 2013.

Lack, D. A. and Corbett, J. J.: Black carbon from ships: a review of the effects of ship speed, fuel quality and exhaust gas scrubbing, Atmos. Chem. Phys., 12, 3985–4000, https://doi.org/10.5194/acp-12-3985-2012, 2012.

Lack, D. A., Corbett, J. J., Onasch, T., Lerner, B., Massoli, P., Quinn, P. K., Bates, T. S., Covert, D. S., Coffman, D., Sierau, B., Herndon, S., Allan, J., Baynard, T., Lovejoy, E., Ravishankara, A. R., and Williams, E.: Particulate emissions from commercial shipping: Chemical, physical, and optical properties, J. Geophys. Res.-Atmos., 114, 1–16, https://doi.org/10.1029/2008JD011300, 2009.

Lack, D. A., Cappa, C. D., Langridge, J., Bahreini, R., Buffaloe, G., Brock, C., Cerully, K., Coffman, D., Hayden, K., Holloway, J., Lerner, B., Massoli, P., Li, S.-M., McLaren, R., Middlebrook, A. M., Moore, R., Nenes, A., Nuaaman, I., Onasch, T. B., Peischl, J., Perring, A., Quinn, P. K., Ryerson, T., Schwartz, J. P., Spackman, R., Wofsy, S. C., Worsnop, D., Xiang, B., and Williams, E.: Impact of Fuel Quality Regulation and Speed Reductions on Shipping Emissions: Implications for Climate and Air Quality, Environ. Sci. Technol., 45, 9052–9060, https://doi.org/10.1021/es2013424, 2011.

Lasserre, F. and Pelletier, S.: Polar super seaways? Maritime transport in the Arctic: an analysis of shipowners' intentions, J. Transp. Geogr., 19, 1465–1473, https://doi.org/10.1016/j.jtrangeo.2011.08.006, 2011.

Lauer, A., Eyring, V., Hendricks, J., Jöckel, P., and Lohmann, U.: Global model simulations of the impact of ocean-going ships on aerosols, clouds, and the radiation budget, Atmos. Chem. Phys., 7, 5061–5079, https://doi.org/10.5194/acp-7-5061-2007, 2007.

Lehtoranta, K., Aakko-Saksa, P., Murtonen, T., Vesala, H., Ntziachristos, L., Rönkkö, T., Karjalainen, P., Kuittinen, N., and Timonen, H.: Particulate Mass and Nonvolatile Particle Number Emissions from Marine Engines Using Low-Sulfur Fuels, Natural Gas, or Scrubbers, Environ. Sci. Technol., 53, 3315–3322, https://doi.org/10.1021/acs.est.8b05555, 2019.

Li, X., Lynch, A. H., Bailey, D. A., Stephenson, S. R., and Veland, S.: The impact of black carbon emissions from projected Arctic shipping on regional ice transport, Clim. Dynam., 57, 2453–2466, https://doi.org/10.1007/s00382-021-05814-9, 2021.

Lieke, K. I., Rosenørn, T., Pedersen, J., Larsson, D., Kling, J., Fuglsang, K., and Bilde, M.: Micro- and Nanostructural Characteristics of Particles Before and After an Exhaust Gas Recirculation System Scrubber, Aerosol Sci. Tech., 47, 1038–1046, https://doi.org/10.1080/02786826.2013.813012, 2013.

Liu, H., Fu, M., Jin, X., Shang, Y., Shindell, D., Faluvegi, G., Shindell, C., and He, K.: Health and climate impacts of ocean-going vessels in East Asia, Nat. Clim. Change, 6, 1037–1041, https://doi.org/10.1038/nclimate3083, 2016.

Lund, M. T., Eyring, V., Fuglestvedt, J., Hendricks, J., Lauer, A., Lee, D., and Righi, M.: Global-Mean Temperature Change from Shipping toward 2050: Improved Representation of the Indirect Aerosol Effect in Simple Climate Models, Environ. Sci. Technol., 46, 8868–8877, https://doi.org/10.1021/es301166e, 2012.

Lund, M. T., Aamaas, B., Stjern, C. W., Klimont, Z., Berntsen, T. K., and Samset, B. H.: A continued role of short-lived climate

forcers under the Shared Socioeconomic Pathways, Earth Syst. Dynam., 11, 977–993, https://doi.org/10.5194/esd-11-977-2020, 2020.

Mahrt, F., Marcolli, C., David, R. O., Grönquist, P., Barthazy Meier, E. J., Lohmann, U., and Kanji, Z. A.: Ice nucleation abilities of soot particles determined with the Horizontal Ice Nucleation Chamber, Atmos. Chem. Phys., 18, 13363–13392, https://doi.org/10.5194/acp-18-13363-2018, 2018.

Manshausen, P., Watson-Parris, D., Christensen, M. W., Jalkanen, J.-P., and Stier, P.: Invisible Ship Tracks Show Large Cloud Sensitivity to Aerosol, Nature, 610, 101–106, https://doi.org/10.1038/s41586-022-05122-0, 2022.

Mauritsen, T., Sedlar, J., Tjernström, M., Leck, C., Martin, M., Shupe, M., Sjogren, S., Sierau, B., Persson, P. O. G., Brooks, I. M., and Swietlicki, E.: An Arctic CCN-limited cloud-aerosol regime, Atmos. Chem. Phys., 11, 165–173, https://doi.org/10.5194/acp-11-165-2011, 2011.

Meador, W. E. and Weaver, W. R.: Two-Stream Approximations to Radiative Transfer in Planetary Atmospheres: A Unified Description of Existing Methods and a New Improvement, J. Atmos. Sci., 37, 630–643, https://doi.org/10.1175/1520-0469(1980)037<0630:TSATRT>2.0.CO;2, 1980.

Morrison, H., De Boer, G., Feingold, G., Harrington, J., Shupe, M. D., and Sulia, K.: Resilience of persistent Arctic mixed-phase clouds, Nat. Geosci., 5, 11–17, https://doi.org/10.1038/ngeo1332, 2012.

Oikawa, K., Yongsiri, C., Takeda, K., and Harimoto, T.: Seawater flue gas desulfurization: Its technical implications and performance results, Environ. Prog., 22, 67–73, https://doi.org/10.1002/ep.670220118, 2003.

Ovchinnikov, M., Korolev, A., and Fan, J.: Effects of ice number concentration on dynamics of a shallow mixed-phase stratiform cloud, J. Geophys. Res., 116, D00T06, https://doi.org/10.1029/2011JD015888, 2011.

Ovchinnikov, M., Ackerman, A. S., Avramov, A., Cheng, A., Fan, J., Fridlind, A. M., Ghan, S., Harrington, J., Hoose, C., Korolev, A., McFarquhar, G. M., Morrison, H., Paukert, M., Savre, J., Shipway, B. J., Shupe, M. D., Solomon, A., and Sulia, K.: Intercomparison of large-eddy simulations of Arctic mixed-phase clouds: Importance of ice size distribution assumptions, J. Adv. Model. Earth Sy., 6, 223–248, https://doi.org/10.1002/2013MS000282, 2014.

Paxian, A., Eyring, V., Beer, W., Sausen, R., and Wright, C.: Present-day and future global bottom-up ship emission inventories including polar routes, Environ. Sci. Technol., 44, 1333–1339, https://doi.org/10.1021/es9022859, 2010.

Peters, G. P., Nilssen, T. B., Lindholt, L., Eide, M. S., Glomsrød, S., Eide, L. I., and Fuglestvedt, J. S.: Future emissions from shipping and petroleum activities in the Arctic, Atmos. Chem. Phys., 11, 5305–5320, https://doi.org/10.5194/acp-11-5305-2011, 2011.

Petters, M. D. and Kreidenweis, S. M.: A single parameter representation of hygroscopic growth and cloud condensation nucleus activity, Atmos. Chem. Phys., 7, 1961–1971, https://doi.org/10.5194/acp-7-1961-2007, 2007.

Petzold, A., Hasselbach, J., Lauer, P., Baumann, R., Franke, K., Gurk, C., Schlager, H., and Weingartner, E.: Experimental studies on particle emissions from cruising ship, their characteristic properties, transformation and atmospheric lifetime in the marine boundary layer, Atmos. Chem. Phys., 8, 2387–2403, https://doi.org/10.5194/acp-8-2387-2008, 2008.

Possner, A., Ekman, A. M. L., and Lohmann, U.: Cloud response and feedback processes in stratiform mixed-phase clouds perturbed by ship exhaust, Geophys. Res. Lett., 44, 1964–1972, https://doi.org/10.1002/2016GL071358, 2017.

Possner, A., Wang, H., Wood, R., Caldeira, K., and Ackerman, T. P.: The efficacy of aerosol–cloud radiative perturbations from near-surface emissions in deep open-cell stratocumuli, Atmos. Chem. Phys., 18, 17475–17488, https://doi.org/10.5194/acp-18-17475-2018, 2018.

Rantanen, M., Karpechko, A. Y., Lipponen, A., Nordling, K., Hyvärinen, O., Ruosteenoja, K., Vihma, T., and Laaksonen, A.: The Arctic has warmed nearly four times faster than the globe since 1979, Communications Earth & Environment, 3, 168, https://doi.org/10.1038/s43247-022-00498-3, 2022.

Roberts, G. C. and Nenes, A.: A Continuous-Flow Streamwise Thermal-Gradient CCN Chamber for Atmospheric Measurements, Aerosol Sci. Tech., 39, 206–221, https://doi.org/10.1080/027868290913988, 2005.

Santos, L. F. E. d., Salo, K., and Thomson, E. S.: Quantification and physical analysis of nanoparticle emissions from a marine engine using different fuels and a laboratory wet scrubber, Environ. Sci.-Proc. Imp., 24, 1769–1781, https://doi.org/10.1039/D2EM00054G, 2022.

Santos, L. F. E. d., Salo, K., Kong, X., Noda, J., Kristensen, T. B., Ohigashi, T., and Thomson, E. S.: Changes in CCN activity of ship exhaust particles induced by fuel sulfur content reduction and wet scrubbing, Environmental Science: Atmospheres, 3, 182–195, https://doi.org/10.1039/D2EA00081D, 2023.

Santos, L. F. E. D., Salo, K., Kong, X., Hartmann, M., Sjöblom, J., and Thomson, E. S.: Marine Fuel Regulations and Engine Emissions: Impacts on Physicochemical Properties, Cloud Activity and Emission Factors, J. Geophys. Res.-Atmos., 129, e2023JD040389, https://doi.org/10.1029/2023JD040389, 2024.

Savre, J., Ekman, A. M. L., and Svensson, G.: Technical note: Introduction to MIMICA, a large-eddy simulation solver for cloudy planetary boundary layers, J. Adv. Model. Earth Sy., 6, 630–649, https://doi.org/10.1002/2013MS000292, 2014.

Savre, J., Ekman, A. M. L., Svensson, G., and Tjernström, M.: Large-eddy simulations of an Arctic mixed-phase stratiform cloud observed during ISDAC: sensitivity to moisture aloft, surface fluxes and large-scale forcing, Q. J. Roy. Meteor. Soc., 141, 1177–1190, https://doi.org/10.1002/qj.2425, 2015.

Schmale, J., Zieger, P., and Ekman, A. M. L.: Aerosols in current and future Arctic climate, Nature Climate Change, 11, 95–105, https://doi.org/10.1038/s41558-020-00969-5, 2021.

Screen, J. A. and Simmonds, I.: The central role of diminishing sea ice in recent Arctic temperature amplification, Nature, 464, 1334–1337, https://doi.org/10.1038/nature09051, 2010.

Seifert, A. and Beheng, K. D.: A double-moment parameterization for simulating autoconversion, accretion and selfcollection, Atmos. Res., 59-60, 265–281, https://doi.org/10.1016/S0169-8095(01)00126-0, 2001.

Seifert, A. and Beheng, K. D.: A Two-Moment Cloud Microphysics Parameterization for Mixed-Phase Clouds. Part 1: Model Description, Meteorol. Atmos. Phys., 92, 45–66, https://doi.org/10.1007/s00703-005-0112-4, 2006.

Seppälä, S. D., Kuula, J., Hyvärinen, A.-P., Saarikoski, S., Rönkkö, T., Keskinen, J., Jalkanen, J.-P., and Timonen, H.: Effects of marine fuel sulfur restrictions on particle number concentrations and size distributions in ship plumes in the Baltic Sea, Atmos. Chem. Phys., 21, 3215–3234, https://doi.org/10.5194/acp-21-3215-2021, 2021.

Serreze, M. C. and Barry, R. G.: Processes and impacts of Arctic amplification: A research synthesis, Global Planet. Change, 77, 85–96, https://doi.org/10.1016/j.gloplacha.2011.03.004, 2011.

Serreze, M. C. and Francis, J. A.: The Arctic Amplification Debate, Climatic Change, 76, 241–264, https://doi.org/10.1007/s10584-005-9017-y, 2006.

Shupe, M. D. and Intrieri, J. M.: Cloud Radiative Forcing of the Arctic Surface: The Influence of Cloud Properties, Surface Albedo, and Solar Zenith Angle, J. Climate, 17, 616–628, https://doi.org/10.1175/1520-0442(2004)017<0616:CRFOTA>2.0.CO;2, 2004.

Smith, L. C. and Stephenson, S. R.: New Trans-Arctic shipping routes navigable by midcentury, P. Natl. Acad. Sci. USA, 110, E1191–E1195, https://doi.org/10.1073/pnas.1214212110, 2013.

Sotiropoulou, G., Ickes, L., Nenes, A., and Ekman, A. M. L.: Ice multiplication from ice–ice collisions in the high Arctic: sensitivity to ice habit, rimed fraction, ice type and uncertainties in the numerical description of the process, Atmos. Chem. Phys., 21, 9741–9760, https://doi.org/10.5194/acp-21-9741-2021, 2021.

Stephens, G. L.: Radiation Profiles in Extended Water Clouds. II: Parameterization Schemes, J. Atmos. Sci., 35, 2123–2132, 1978.

Stephenson, S. R., Wang, W., Zender, C. S., Wang, H., Davis, S. J., and Rasch, P. J.: Climatic Responses to Future Trans-Arctic Shipping, Geophys. Res. Lett., 45, 9898–9908, https://doi.org/10.1029/2018GL078969, 2018.

Stevens, R. G., Loewe, K., Dearden, C., Dimitrelos, A., Possner, A., Eirund, G. K., Raatikainen, T., Hill, A. A., Shipway, B. J., Wilkinson, J., Romakkaniemi, S., Tonttila, J., Laaksonen, A., Korhonen, H., Connolly, P., Lohmann, U., Hoose, C., Ekman, A. M. L., Carslaw, K. S., and Field, P. R.: A model intercomparison of CCN-limited tenuous clouds in the high Arctic, Atmos. Chem. Phys., 18, 11041–11071, https://doi.org/10.5194/acp-18-11041-2018, 2018.

Tavakoli, F. and Olfert, J. S.: Determination of particle mass, effective density, mass-mobility exponent, and dynamic shape factor using an aerodynamic aerosol classifier and a differential mobility analyzer in tandem, J. Aerosol Sci., 75, 35–42, https://doi.org/10.1016/j.jaerosci.2014.04.010, 2014.

Taylor, P. C. and Monroe, E.: Isolating the Surface Type Influence on Arctic Low-Clouds, J. Geophys. Res.-Atmos., 128, e2022JD038098, https://doi.org/10.1029/2022JD038098, 2023.

Tjernström, M., Birch, C. E., Brooks, I. M., Shupe, M. D., Persson, P. O. G., Sedlar, J., Mauritsen, T., Leck, C., Paatero, J., Szczodrak, M., and Wheeler, C. R.: Meteorological conditions in the central Arctic summer during the Arctic Summer Cloud Ocean Study (ASCOS), Atmos. Chem. Phys., 12, 6863–6889, https://doi.org/10.5194/acp-12-6863-2012, 2012.

Tjernström, M., Leck, C., Birch, C. E., Bottenheim, J. W., Brooks, B. J., Brooks, I. M., Bäcklin, L., Chang, R. Y.-W., de Leeuw, G., Di Liberto, L., de la Rosa, S., Granath, E., Graus, M., Hansel, A., Heintzenberg, J., Held, A., Hind, A., Johnston, P., Knulst, J., Martin, M., Matrai, P. A., Mauritsen, T., Müller, M., Norris, S. J., Orellana, M. V., Orsini, D. A., Paatero, J., Persson, P. O. G., Gao, Q., Rauschenberg, C., Ristovski, Z., Sedlar, J., Shupe, M. D., Sierau, B., Sirevaag, A., Sjogren, S., Stetzer, O., Swietlicki, E., Szczodrak, M., Vaattovaara, P., Wahlberg, N., Westberg, M., and Wheeler, C. R.: The Arctic Summer Cloud Ocean Study (ASCOS): overview and experimental design, Atmos. Chem. Phys., 14, 2823–2869, https://doi.org/10.5194/acp-14-2823-2014, 2014.

UNCTAD: Review of Maritime Transport 2023, no. 2022 in Review of maritime transport/United Nations Conference on Trade and Development, Geneva, United Nations, Geneva, ISBN 978-92-1-002886-8, 2022.

Wang, C. and Chang, J. S.: A three-dimensional numerical model of cloud dynamics, microphysics, and chemistry: 1. Concepts and formulation, J. Geophys. Res.-Atmos., 98, 14827–14844, https://doi.org/10.1029/92JD01393, 1993.

Watson-Parris, D., Christensen, M. W., Laurenson, A., Clewley, D., Gryspeerdt, E., and Stier, P.: Shipping Regulations Lead to Large Reduction in Cloud Perturbations, P. Natl. Acad. Sci. USA, 119, e2206885119, https://doi.org/10.1073/pnas.2206885119, 2022.

Winnes, H., Fridell, E., and Moldanová, J.: Effects of Marine Exhaust Gas Scrubbers on Gas and Particle Emissions, J. Mar. Sci. Eng., 8, 299, https://doi.org/10.3390/jmse8040299, 2020.

Yang, J., Tang, T., Jiang, Y., Karavalakis, G., Durbin, T. D., Wayne Miller, J., Cocker, D. R., and Johnson, K. C.: Controlling emissions from an ocean-going container vessel with a wet scrubber system, Fuel, 304, 121323, https://doi.org/10.1016/j.fuel.2021.121323, 2021.

Yu, C., Pasternak, D., Lee, J., Yang, M., Bell, T., Bower, K., Wu, H., Liu, D., Reed, C., Bauguitte, S., Cliff, S., Trembath, J., Coe, H., and Allan, J. D.: Characterizing the Particle Composition and Cloud Condensation Nuclei from Shipping Emission in Western Europe, Environ. Sci. Technol., 54, 15604–15612, https://doi.org/10.1021/acs.est.0c04039, 2020.

Yu, C., Pasternak, D., Lee, J., Yang, M., Bell, T., Bower, K., Wu, H., Liu, D., Reed, C., Bauguitte, S., Cliff, S., Trembath, J., Coe, H., and Allan, J. D.: Correction to "Characterizing the Particle Composition and Cloud Condensation Nuclei from Shipping Emission in Western Europe", Environ. Sci. Technol., 57, 7888–7889, https://doi.org/10.1021/acs.est.3c03005, 2023.

Yuan, T., Song, H., Wood, R., Wang, C., Oreopoulos, L., Platnick, S. E., von Hippel, S., Meyer, K., Light, S., and Wilcox, E.: Global Reduction in Ship-Tracks from Sulfur Regulations for Shipping Fuel, Sci. Adv., 8, eabn7988, https://doi.org/10.1126/sciadv.abn7988, 2022.

Zetterdahl, M., Moldanová, J., Pei, X., Pathak, R. K., and Demirdjian, B.: Impact of the 0.1 % fuel sulfur content limit in SECA on particle and gaseous emissions from marine vessels, Atmos. Environ., 145, 338–345, https://doi.org/10.1016/j.atmosenv.2016.09.022, 2016.